Research Article

Sonic hedgehog is basolaterally sorted from the TGN and transcytosed to the apical domain involving Dispatched-1 at Rab11-ARE

Lisette Sandoval[1, #], Mariana Labarca[1, #], Claudio Retamal[1], Paula Sanchez[2], Juan Larraín[2], Alfonso González[1,2,3]

[1]Centro de Biología Celular y Biomedicina (CEBICEM), Facultad de Medicina y Ciencia, Universidad San Sebastián, Santiago 7510157, Chile. [2]Centro de Envejecimiento y Regeneración (CARE), Facultad de Ciencias Biológicas, Pontificia Universidad Católica de Chile, Santiago 8330025, Chile. [3]Fundación Ciencia y Vida, Santiago 7780272, Chile.

[#] These authors contributed equally and are considered first authors

Keywords: Hedgehog, polarity, trafficking, dispatched, Rab11, lipidation.

The authors declare no conflicts of interest

Corresponding author: Alfonso González
Centro de Biología Celular y Biomedicina (CEBICEM)
Facultad de Medicina y Ciencia
Universidad San Sebastián
Santiago 7510157, Chile
E-mail: alfonso.gonzalez@uss.cl
Phone: +56 2 22606300

ABSTRACT

Hedgehog (Hh) secretion from apical and/or basolateral domains occurs in different epithelial cells impacting development and tissue homeostasis. Palmitoylation and cholestyrolation attach Hh proteins to membranes and Dispatched-1 (Disp-1) promotes their release. How these lipidated proteins are handled by the complex secretory and endocytic pathways of polarized epithelial cells remains unknown. We show that MDCK cells address newly synthesized sonic hedgehog (Shh) from the TGN to the basolateral cell surface and then to the apical domain through a transcytosis pathway that includes Rab11-apical recycling endosomes (Rab11-ARE). Both palmitoylation and cholestyrolation contribute to this sorting behavior, otherwise Shh lacking these lipid modifications is unpolarized. Disp-1 mediates first basolateral secretion from the TGN and then transcytosis from the Rab11-ARE. At steady state, Shh predominates apically and can be basolaterally transcytosed. This complex Shh trafficking provides several steps for regulation and variation in different epithelia, subordinating the apical to the basolateral secretion.

45 **INTRODUCTION**

46 Hedgehog proteins (Hhs) are signaling determinants of embryonic patterning,
47 differentiation and organogenesis and after birth contribute to tissue homeostasis and repair
48 (Beachy et al., 2004; Briscoe and Therond, 2013; Guerrero and Kornberg, 2014; Parchure et
49 al., 2018; Petrov et al., 2017). Alterations of Hhs functions are involved in developmental
50 defects, tissue fibrosis and cancer (Briscoe and Therond, 2013; Edeling et al., 2016; Machado
51 and Diehl, 2017). In most of these processes the function of Hhs depends on polarized
52 secretion from epithelial cells that possess apical and basolateral domains facing opposite
53 compartments of the organism (Briscoe and Therond, 2013; Guerrero and Kornberg, 2014; Mao
54 et al., 2018; Matusek et al., 2020; Parchure et al., 2018; Peng et al., 2015; Petrov et al., 2017;
55 Walton and Gumucio, 2021). Apical secretion sends signals to neighboring epithelial cells while
56 basolateral secretion targets neighboring epithelial cells and underlying stromal cells
57 (Chamberlain et al., 2008; Lehmann et al., 2020; Mao et al., 2018; Walton and Gumucio, 2021).
58 Elucidating the Hhs intracellular trafficking pathways in epithelial cells is then required to fully
59 understand the signaling function of these important morphogens in development, tissue
60 homeostasis and pathology.

61 Hhs are synthesized in the endoplasmic reticulum (ER) as a 45kD precursor that is
62 autocatalytically cleaved and processed, generating a ~20kDa N-terminal peptide modified by
63 the covalent addition of cholesterol to its C-terminus and palmitate to its N-terminal end (Chen
64 et al., 2011; Pepinsky et al., 1998; Porter et al., 1996). These lipid moieties attach the mature
65 and functionally competent Hhs to the membrane (Petrov et al., 2017). Multiple forms of Hhs
66 secretion have been described, including oligomers, lipoproteins, exosomes and a main
67 releasing mechanism from the plasma membrane involving the transmembrane and cholesterol
68 binding protein Dispatched (Disp) (Burke et al., 1999; Caspary et al., 2002; Creanga et al.,
69 2012; Parchure et al., 2018; Stewart et al., 2018; Tukachinsky et al., 2012). Disp functions as
70 Hhs/Na+ antiporter driven by the Na+ gradient (Petrov et al., 2020; Wang et al., 2021) and
71 becomes functionally competent after its cleavage at the cell surface by the proprotein
72 convertase Furin, which in epithelial cells occurs at the basolateral plasma membrane (Hall et
73 al., 2019; Stewart et al., 2018).

74 In different epithelial cells Hhs can be found localized to the apical, basolateral or both
75 plasma membrane domains and their polarized secretion can be inferred from target cell

responses. Sonic hedgehog (Shh), the most studied vertebrate orthologs of Hhs (Parchure et al., 2018; Petrov et al., 2017), generates paracrine responses of stromal mesenchymal cells underneath the epithelial cells of adult intestine (Buller et al., 2012; Shyer et al., 2015), lung (Mao et al., 2018; Peng et al., 2015), and kidney (Ding et al., 2012; Edeling et al., 2016; Zhou et al., 2014), indicating basolateral secretion. Instead, gastric parietal cells distribute and secrete Shh mostly apically, showing also detectable levels at the basolateral side (Zavros et al., 2008). Apically secreted Shh is also found in the neural tube of chick (Danesin et al., 2006) and mouse (Chamberlain et al., 2008) embryos. In the mature airway epithelia, Shh is secreted from both apical and basolateral domains, eliciting different signaling pathways and functional consequences at each compartment (Mao et al., 2018).

The routes followed by Hhs along the complex vesicular trafficking pathways of epithelial cells have been mainly explored in *Drosophila* (Guerrero and Kornberg, 2014; Therond, 2012). Extensive studies interpreting subcellular localizations in producing cells and responses of target cells describe both apical and basolateral pools of Hh and propose a primary biosynthetic pathway to the apical domain, followed by endocytosis and either apical recycling (D'Angelo et al., 2015) or transcytosis of Hh to the basolateral domain (Callejo et al., 2011). These alternative pathways remain highly debated and would determine different secretion and signaling characteristics (Gore et al., 2021; Matusek et al., 2020; Simon et al., 2016). How extensive these *Drosophila* models are to mammalian epithelial cells is unknown.

The biosynthetic routes of different epithelial cells display variations reflecting plasticity in the polarity program (Rodriguez-Boulan and Macara, 2014). Exocytic pathways emerging from the TGN can predominate towards the basolateral domain, from where apical proteins then undergo transcytosis, as in intestinal cells and hepatocytes (Bartles et al., 1987; Hauri and Matter, 1991; Rindler and Traber, 1988; Tuma and Hubbard, 2003). In other epithelial cells, epitomized by kidney epithelial cells, apical and basolateral proteins are first sorted at the TGN into distinct polarized secretion pathways of equivalent transport capacity and endocytic proteins can then recycle to the same or the opposite cell surface (Gonzalez and Rodriguez-Boulan, 2009; Mellman and Nelson, 2008; Rodriguez-Boulan and Macara, 2014; Tuma and Hubbard, 2003). Protein trafficking along polarized vesicular pathways is controlled by sorting signals embedded in the cargo and decoded by a complex machinery coupled to the generation of vesicular/tubular vehicles (Rodriguez-Boulan and Macara, 2014). Transmembrane proteins

107 can have apical sorting signals in extracellular, membrane-spanning or cytosolic domains, or
108 basolateral signals located in their cytosolic domains (Bonifacino, 2014; Gonzalez and
109 Rodriguez-Boulan, 2009; Mellman and Nelson, 2008; Rodriguez-Boulan and Macara, 2014).
110 Luminal proteins anchored to membranes through lipid moieties, such as Hh proteins and
111 glycosylphosphatidylinositol-anchored proteins (GPI-APs), associate with lipid rafts (Long et al.,
112 2015; Parchure et al., 2018; Petrov et al., 2017), originally proposed as platforms for apical
113 sorting (Simons and Ikonen, 1997). Although most GPI-APs are addressed to the apical cell
114 surface, there are also examples of basolateral sorting of GPI-APs associated with lipid-rafts
115 (Imjeti et al., 2011; Lebreton et al., 2021; Lebreton et al., 2019; Paladino et al., 2015; Sezgin et
116 al., 2017). Previous studies describe Hhs subcellular distributions and secretion at steady-state
117 conditions that do not define the trafficking pathways followed by newly synthesized Hhs
118 proteins in epithelial cells.

119 Madin-Darby canine kidney (MDCK) cells forming polarized monolayers in culture
120 constitute the most characterized model system for studies of protein trafficking in epithelial
121 cells (Rodriguez-Boulan and Macara, 2014). In MDCK cells, proteins lacking polarity sorting
122 signals are distributed unpolarized, reflecting TGN-derived apical and basolateral routes of
123 equivalent capacity (Gonzalez et al., 1987; Gottlieb et al., 1986), whereas domain-selective
124 secretion implies specific sorting events occurring at the TGN (Gonzalez et al., 1993; Scheiffele
125 et al., 1995). A unique study in transfected MDCK cells describes Shh steady-state apical and
126 basolateral distribution and enhanced basolateral secretion by coexpressed Disp-1 (Etheridge
127 et al., 2010). This study leaves uncertainty as to whether Shh basolateral secretion occurred
128 directly from the TGN or indirectly through transcytosis from the apical domain, as suggested in
129 Drosophila (Callejo et al., 2011).

130 A combination of experimental approaches previously used for GPI-APs (Paladino et
131 al., 2006; Zurzolo et al., 1993), transmembrane (Cancino et al., 2007; Gan et al., 2002; Kreitzer
132 et al., 2000) and secretion (Gonzalez et al., 1987) proteins can be applied to define the
133 biosynthetic and endocytic trafficking routes of newly synthesized Shh. Here we evaluate Shh
134 trafficking in MDCK cells using pulse-chase domain-specific targeting assays (Cancino et al.,
135 2007; Paladino et al., 2006), plasmid microinjection expression combined with synchronized
136 post-TGN trafficking imaging of Shh, co-expression with Disp1 in live cells (Cancino et al., 2007;
137 Kreitzer et al., 2003), and cell surface tagging with biotin or antibody. The results reveal that

138 newly synthesized Shh is first sorted from the TGN to the basolateral plasma membrane and
139 then undergo transcytosis to the apical cell surface involving the Rab11-apical recycling
140 endosome (Rab11-ARE). Shh polarized sorting requires the lipid modifications and therefore
141 depends on membrane association. At steady state, Shh is mainly localized at the apical cell
142 surface and its secretion is also mainly apical. A small proportion recycles back to the
143 basolateral cell surface. We also show that Disp-1 first promotes basolateral secretion of newly
144 synthesized Shh transported from the TGN and then is required for its transcytosis through the
145 Rab11-ARE to the apical domain. Such a complex trafficking behavior predicts that apical Shh
146 secretion reciprocally depends on previous basolateral secretion and transcytosis processes
147 that are both sensitive to Disp-1 cleavage and expression levels.
148

149 **RESULTS**

150 ***Predominant apical distribution and secretion of Sonic Hedgehog in polarized***
151 ***epithelial MDCK cells***

152 Previous studies indicate that Shh can be found distributed at and secreted from apical
153 and basolateral domains with variable preponderance in different epithelial cells (Briscoe and
154 Therond, 2013; Chamberlain et al., 2008; Guerrero and Kornberg, 2014; Mao et al., 2018;
155 Petrov et al., 2017; Shyer et al., 2015; Zavros et al., 2008; Zhou et al., 2014). To explore the
156 trafficking behavior of Shh in a widely characterized epithelial model system (Mellman and
157 Nelson, 2008; Rodriguez-Boulan and Macara, 2014), we generated permanently transfected
158 MDCK cells expressing different levels of Shh and first assessed the polarity of Shh distribution
159 and secretion at steady state conditions. Domain-specific cell surface biotinylation of MDCK-
160 Shh cells grown in Transwell chambers revealed Shh either highly polarized at the apical
161 domain or unpolarized, depending on its expression levels (Figure 1A). For instance, MDCK-
162 Shh clone-1 distributed Shh mainly apically whereas the MDCK-Shh clone-2 displaying higher
163 expression levels displayed Shh similarly at apical and basolateral cell surfaces. E-cadherin and
164 Na-K-ATPase, two basolateral proteins, demonstrated that both MDCK clones are polarized
165 (Figure 1A). Treatment of MDCK-Shh clone 1 with Na^+-butyrate treatment, known to enhance
166 the expression of transfected plasmids (Burgos et al., 2004; Gonzalez et al., 1987), led to a loss
167 of the predominant apical Shh location, while maintaining the polarity of endogenous E-cadherin
168 Na^+-K^+-ATPase (Figure 1A). These results indicate a predominant apical sorting of Shh through
169 a process that can be saturated at high expression levels. We then focused on MDCK-Shh
170 clone-1, named afterwards as MDCK-Shh, which mainly distributed Shh apically. A quantitative
171 assessment showed ~80% Shh distribution at the apical cell surface and more than 90% apical
172 secretion of Shh in this clone (Figure 1B). The predominant apical pattern of Shh can be also
173 observed by indirect immunofluorescence (Figure 1C).

174 ***Shh is basolaterally sorted and then transcytosed to the apical cell surface***

175 Shh is known to associate with lipid rafts (Long et al., 2015; Parchure et al., 2018;
176 Petrov et al., 2017), similar to GPI-APs, which in general are mainly addressed to the apical
177 domain from the TGN (Hua et al., 2006; Paladino et al., 2006). Therefore, to test whether newly
178 synthesized Shh is directly sorted to the apical cell surface or follows an indirect basolateral-to-
179 apical transcytotic route we pulse-labeled MDCK-Shh cells with [^{35}S]-methionine/cysteine and

180 then chased the arrival of newly synthesized [^{35}S]-Shh to the apical and basolateral cell
181 surfaces using an established biotinylation targeting assay (Le Bivic et al., 1989; Zurzolo et al.,
182 1992). This approach showed that [^{35}S]-Shh first became enriched at the basolateral surface
183 and then progressively increased at the apical cell surface (Figure 2A). E-cadherin used as
184 internal control displayed a basolateral distribution at all chased times. In contrast with Shh,
185 GFP-NO-GPI distributed mostly to the apical cell surface at all chased times (Figure 2B),
186 indicating that our targeting assay is able to detect the TGN-to-apical cell surface pathway
187 previously described for raft-associated GPI-APs in MDCK cells (Imjeti et al., 2011). We also
188 found [^{35}S]-Shh in the apical media after 120 minutes of chase, while basolateral secretion was
189 barely detectable (Figure 2C). These results suggest that newly synthesized Shh is primarily
190 sorted to the basolateral domain from the TGN and then is transported by transcytosis to the
191 apical cell surface.

192 To directly test basolateral-to-apical transcytosis, we first performed an established
193 assay based on the reducible reagent sulfo-NHS-SS-biotin (Burgos et al., 2004; Zurzolo et al.,
194 1992). After 120 min of transport from the biotinylated basolateral cell surface, approximately
195 25% of Shh became protected from reduction by MesNa added to the basolateral chamber
196 (Figure 2D). MesNa added to the apical side also decreased the biotinylation levels of
197 basolaterally biotinylated Shh, but not E-cadherin (Figure 2D). Furthermore, we also found in
198 the apical media Shh previously biotinylated from the basolateral cell surface (Figure 2E).
199 These results indicate that Shh already present at the basolateral cell surface reaches the
200 apical cell surface and is apically secreted by transcytosis.

201 We further corroborate these findings and analyze the route of Shh to the apical domain
202 we tagged the basolateral pool of Shh with anti-Shh antibodies at 4ºC and then shifted the cells
203 to 37ºC for different times. The basolateral pattern of antibody-tagged Shh (0 min) changed
204 within 60 min to a dot-like pattern typical of the apical recycling endosomes (ARE) and then
205 acquired an apical pattern (Figure 3A). Colocalization of Shh with Rab11 indicated that the
206 subapical dot-like compartment actually corresponds to Rab11-ARE (Figure 3B). Therefore,
207 basolaterally sorted Shh follows the well-known transcytotic route widely characterized for the
208 polyimmunoglobulin (PIgR), which includes the Rab11- ARE (Apodaca et al., 1994; Brown et
209 al., 2000; Wang et al., 2000).

210 ***Shh can recycle from the apical cell surface back to the basolateral cell surface***

211 Our results so far indicate that newly synthesized Shh follows a transcytotic pathway
212 from the basolateral to the apical membrane. This is congruent with one of the models proposed
213 for Hh protein trafficking in *Drosophila* (Gallet et al., 2003; Gallet et al., 2006). However, the
214 opposite apical-to-basolateral Hh transcytosis has also been proposed in *Drosophila* (Callejo et
215 al., 2011; Guerrero and Kornberg, 2014). Therefore, we used the same type of antibody-tagging
216 experiment and looked for apical-to-basolateral transcytosis. We find that apically tagged Shh
217 can also redistribute to the basolateral cell surface (Figure 3C). Therefore, as suggested in
218 *Drosophila* wing disk epithelia (Callejo et al., 2011; Guerrero and Kornberg, 2014), once arriving
219 to the apical surface Shh can recycle back to the basolateral cell surface by transcytosis.

220 ***Role of lipid modifications in Shh polarized sorting***

221 Hhs proteins are synthesized as a precursor protein that is autocleaved and processed
222 by cholesteroylation at the C-terminus and palmitoylation at the N-terminus (Chen et al., 2011;
223 Pepinsky et al., 1998; Porter et al., 1996) (Figure 4A). These lipid modifications determine Hhs
224 membrane association, nano-scale organization, mode of secretion and range of action
225 (Parchure et al., 2018; Petrov et al., 2017). Therefore, we assessed the polarity of Shh mutants
226 lacking both palmitoylation and cholesterylation (ShhNC24S), only cholesterylation (ShhN) or
227 palmitoylation (ShhNpC24S). ShhNC24S that lacks both lipid modifications and does not
228 associate with membrane (Feng et al., 2004) was secreted without polarity (Figure 4B).
229 Therefore, the peptidic structure of Shh either lacks specific sorting signals for polarity or
230 requires membrane association to expose sorting competent signals, perhaps through nano-
231 scale organization (Vyas et al., 2008; Vyas et al., 2014). We also found the C-terminal truncated
232 mutant ShhN lacking cholesterylation associated to the basolateral cell surface and secreted
233 unpolarized (Figure 4C). Instead, ShhNpC24S lacking the cysteine for palmitoylation and
234 conserving the cholesterol modification preferentially distributed to the basolateral membrane
235 and was mostly secreted apically (Figure 4D). Pulse-chase domain-specific targeting assays
236 showed that newly synthesized ShhNpC24S arrived first at the basolateral cell surface and then
237 at the apical cell surface and medium (Figure 4E), similar to the pathway followed by the fully
238 lapidated protein (See Figure 2A). The low detection levels at the apical cell surface suggest a
239 faster release of this mutant. The transcytosis assay corroborated an apical secretion of
240 basolaterally biotinylated-ShhNpC24S (Figure 4F). These results suggest that ShhNpC24S,
241 similar to wild-type Shh, is initially sorted to the basolateral cell surface and then becomes

242 transcytosed to the apical domain for secretion. All these observations reveal that both palmitoyl
243 and cholesteroyl modifications contribute to Shh sorting to the basolateral cell surface. The
244 cholesterol adduct would be further required for subsequent transcytosis.

245 ***Disp-1 distribution and role in newly synthesized Shh secretion***

246 Disp is required for the release of Hh proteins from expressing cells (Burke et al., 1999;
247 Caspary et al., 2002; Petrov et al., 2017; Stewart et al., 2018). In polarized epithelial cells, Disp
248 has been described to promote Hh basolateral secretion (Callejo et al., 2011; Etheridge et al.,
249 2010; Stewart et al., 2018). We used plasmid microinjection (Cancino et al., 2007; Kreitzer et
250 al., 2003) to express Shh alone or together with HA-tagged Disp-1 (Stewart et al., 2018).
251 Microinjection avoids the high levels of overexpression achieved by transient cotransfection
252 experiments, which can alter polarized sorting (Burgos et al., 2004). After 4 h post-
253 microinjection we clearly found Shh distributed apically, contrasting with the co-expressed
254 basolateral marker LDLR-GFP (Cancino et al., 2007; Gravotta et al., 2007; Guo et al., 2013)
255 (Figure 5A). Using these conditions, we co-expressed Shh together with Disp-1 and incubated
256 the intact cells with anti-Shh added to the apical side to detect Shh at the cell surface. Then we
257 permeabilized the cells for Disp-1 immunodetection and found it localized just below the Shh
258 labeled at the apical cell surface (Figure 5B). In the next experiments, we fixed and
259 permeabilized the cells to immunolocalize Shh and Disp-1 at the same time. Confocal images
260 were then merged and shown as either maximal projections or just a basolateral section at the
261 level of the nucleus (Figure 5C). Shh expressed alone can be seen in its typical apical location
262 Shh (Figure 5C, upper panel), while when co-expressed with Disp-1 also became visible at the
263 basolateral border of neighboring non-microinjected cells (Figure 5C, middle panel). This
264 indicates that Disp-1 enhanced the basolateral secretion of Shh, as previously described
265 (Etheridge et al., 2010). Shh and Disp-1 mostly segregated from each other, with Disp-1
266 occupying a subapical location overlaid by Shh. Both proteins also colocalized in few spots
267 (Figure 5C, middle panel).

268 Then, we co-expressed Shh together with the cleavage deficient recombinant mutant
269 Disp-1-R279A/E280A (Disp-1-CS) incompetent for Shh secretion (Stewart et al., 2018). Disp-1-
270 CS displayed an overall similar distribution as Disp-1. However, Disp-1-CS coexpressing cells
271 showed Shh predominantly at the subapical compartment, likely corresponding to the ARE
272 (Figure 5C, bottom panel), and lost the Shh apical location in expressing cells and its

273 basolateral detection in neighboring cells (Figure 5C, bottom panel). These results suggest that
274 Disp-1-CS not only inhibited Shh secretion from the basolateral surface where Shh first arrived,
275 but also arrested Shh at the ARE, while *en route* to the apical cell surface from the basolateral
276 plasma membrane.

277 Using less amounts of microinjected plasmids to achieve lower levels of expression we
278 detected colocalization of Shh and Disp-1 in the Rab11-ARE compartment, which included
279 tubular structures (Figure 6). High resolution images (3D surface rendering) revealed
280 colocalization of Shh, Disp-1 and Rab11 in the tubular structures of the ARE compartment
281 (Figure 6; middle panel, arrowheads). Even though most of Disp-1 is seen at subapical planes,
282 overexposure of Z confocal planes corresponding to the basolateral volume of the cell clearly
283 showed Disp-1 near the lateral membrane, where few vesicles containing Shh or Rab11 were
284 also detectable (Figure 6, bottom panel).

285 To further analyze the role of Disp-1 upon newly synthesized Shh biosynthetic
286 trafficking we performed live-cell imaging from the TGN to cell surface transport of Shh coupled
287 to GFP (Shh-GFP) (Chamberlain et al., 2008). We first corroborated in plasmid-microinjected
288 MDCK cells for Shh-GFP to acquire an apical distribution (Figure 7A) using the route of Rab-11-
289 ARE (Figure 7B). Then, we followed Shh-GFP trafficking from the TGN to the cell surface in a
290 synchronized manner with previously established methods (Cancino et al., 2007; Guo et al.,
291 2013; Kreitzer et al., 2003). After plasmid microinjection, we incubated the cells for 45 minutes
292 at 37ºC to allow for detectable expression levels and then incubated the cells at 20ºC for 2h to
293 arrest the biosynthetic trafficking at the TGN. At this initial time, Shh-GFP expressed alone or in
294 combination with Disp-1 or Disp-1-CS mutant displayed the perinuclear pattern characteristic of
295 the TGN (Figure 7C, 0 min) (Cancino et al., 2007). Shifting the cells to 37ºC allowed the TGN
296 exit in the presence of cycloheximide to avoid further protein synthesis. Shh-GFP first became
297 detectable at the cell border, reflecting its basolateral arrival, and then progressively acquired
298 an ARE location and the typical apical pattern (Figure 7C). A halo of receiving cells surrounding
299 the expressing cells displayed Shh in their border, revealing the Shh basolateral secretion from
300 producing cells (see also Fig 5C middle panel). This can be seen more clearly in the
301 overexposed image corresponding to 120 min post-TGN trafficking (Figure 7C, middle panel).
302 Cells co-expressing Disp-1 showed an enhanced Shh-GFP basolateral secretion, as judged by
303 the higher intensity and longer distance of the fluorescent borders of neighboring non-

304 expressing cells (Figure 7C, middle panel). These results indicate that post-TGN basolateral
305 secretion of Shh is sensitive to Disp-1 expression levels and provide direct evidence of Shh
306 sorting from the TGN to the basolateral cell surface. In striking contrast, cells co-expressing the
307 Disp-1-CS mutant showed a decreased basolateral distribution in neighboring cells (Figure 7C,
308 lower panel), indicating lower basolateral secretion levels. Furthermore, Shh-GFP accumulated
309 in a punctate compartment suggesting an arrest at the ARE (Figure 7C, lower panel). Taken
310 together, all these experiments indicate that Disp1 promotes Shh secretion first from the
311 basolateral cell surface where it arrives from the TGN. The effects of coexpressing Disp-1-CS
312 corroborate that Shh secretion requires Disp-1 processing by cleavage (Stewart et al., 2018)
313 and suggest that Disp-1 is also required for trafficking along the basolateral-to-apical
314 transcytosis route at the level of the ARE, where Shh accumulates if Disp-1 function is
315 disturbed.
316

317 **DISCUSSION**

318 In diverse epithelial systems, Hhs are found apically and basolaterally distributed and
319 secreted with variable polarity (Chamberlain et al., 2008; Mao et al., 2018; Therond, 2012). An
320 open question is whether Hh subcellular distribution and secretion reflects default-unsorted or
321 specific-sorting trafficking events. The steady-state conditions of previous studies cannot
322 answer this question and have even led to controversial models (Ayers et al., 2010; Callejo et
323 al., 2011; Gallet, 2011; Guerrero and Kornberg, 2014; Therond, 2012). We addressed this
324 problem using MDCK cells as model system and combined pulse chase and live cell imaging to
325 follow the cell surface arrival of newly synthesized Shh, while domain specific cell surface
326 tagging directly assessed transcytosis from each polarized domain. Our results provide new
327 information regarding the intracellular routes taken by newly synthesized Shh, which can help to
328 interpret and understand previous observations in different epithelial systems.

329 We find a predominant (~80%) apical cell surface distribution and secretion of Shh in
330 permanently transfected MDCK cells under steady state conditions. However, pulse-chase
331 domain-specific targeting assays reveal that newly synthesized Shh arrives first to the
332 basolateral cell surface and then to the apical plasma membrane. Live cell imaging after
333 releasing a 20Cº TGN arrest demonstrates Shh basolateral sorting directly from the TGN.
334 Basolateral tagging with biotinylation or antibody binding directly demonstrate transcytosis of
335 basolateral Shh to the apical domain. The transcytosis pathway of Shh includes the Rab11-ARE
336 compartment, similar to the most characterized transcytosis route of pIgR (Apodaca et al., 1994;
337 Rojas and Apodaca, 2002). A reverse transcytosis of Shh from the apical to the basolateral
338 domain can also occur, as shown by apical tagging with antibody. All these observations
339 suggest a model in which newly synthesized Shh is first addressed to the basolateral domain
340 from the TGN and then becomes transported through the Rab11-ARE transcytotic route to the
341 opposite apical domain, from which most of its secretion takes place while a small proportion
342 returns to the basolateral cell surface. Our results imply specific sorting events operating first at
343 the TGN and then at the basolateral plasma membrane.

344 MDCK cells possess apical and basolateral exocytic pathways of roughly equivalent
345 transporting capacity and therefore newly synthesized proteins lacking sorting information would
346 follow these pathways by default resulting in their unpolarized distribution or secretion
347 (Gonzalez et al., 1987; Gottlieb et al., 1986; Scheiffele et al., 1995). In contrast, intestinal

348 epithelial cells and hepatocytes have a prominent basolateral exocytic route into which both
349 basolateral and apical proteins can enter and once reaching the cell surface the apical proteins
350 become transcytosed to the opposite domain (Bartles et al., 1987; Hauri and Matter, 1991;
351 Hubbard, 1989; Rindler and Traber, 1988). Proteins lacking information for TGN-mediated
352 sorting that are unpolarized in MDCK cells can be basolaterally addressed in intestinal cells
353 (Rindler and Traber, 1988). Our results in MDCK cells clearly indicate that Shh possess
354 basolateral sorting information decoded first at the TGN and predicts its primary basolateral cell
355 surface arrival in different epithelial cells.

356 We initially considered that Shh sorting behavior might share similarities with GPI-
357 proteins due to their common association with lipid rafts at the luminal membrane leaflet (Mayor
358 and Riezman, 2004). GPI-proteins are most commonly addressed to the apical cell surface from
359 the TGN in MDCK cells (Imjeti et al., 2011; Lebreton et al., 2019; Lisanti et al., 1988; Paladino
360 et al., 2006). However, our pulse chase experiments revealed basolateral sorting of Shh under
361 the same conditions that corroborated apical biosynthetic trafficking of a previously
362 characterized recombinant GPI-protein (Imjeti et al., 2011). Lipid-raft association is certainly not
363 enough for apical sorting (Lebreton et al., 2019; Paladino et al., 2004). A proposed additional
364 requirement for at least apical GPI-proteins is clustering at the TGN promoted by cholesterol
365 and luminal calcium (Lebreton et al., 2021; Paladino et al., 2004), or glycosylation in some
366 epithelial cells (Imjeti et al., 2011). GPI-proteins lacking this clustering property, such as the
367 prion protein, are instead addressed to the basolateral domain (Lebreton et al., 2021; Sarnataro
368 et al., 2002). Prion also becomes transcytosed from the basolateral to the apical domain
369 (Arkhipenko et al., 2016), similar to what we found here for Shh. The mechanism through which
370 lipid-raft associated proteins are basolaterally sorted, endocytosed and addressed to the
371 opposite domain by transcytosis remains unknown.

372 Epithelial cells have transcytosis pathways from the apical or basolateral domains to the
373 opposite cell surface (Mostov et al., 1995; Tuma and Hubbard, 2003). Transmembrane proteins
374 can follow these pathways guided by specific sorting signals or associated with default
375 movement of membranes. For instance, the cytosolic tail of pIgR contains sorting signals for
376 basolateral delivery, clathrin-mediated endocytosis and transcytosis (Luton et al., 2009; Mostov
377 et al., 1995), whereas the basolateral recycling transferrin receptor reaches the apical domain
378 when cells do not express the AP1B-adaptor responsible for its basolateral sorting (Perez Bay

379 et al., 2013), suggesting a default post-endocytic trafficking. Both pathways include transit
380 through the Rab11-ARE compartment (Luton et al., 2009; Mostov et al., 1995; Perez Bay et al.,
381 2013). We show that Shh still associated with the basolateral plasma membrane moves towards
382 the apical cell surface using the Rab11-ARE transcytotic route. The mechanism might involve
383 yet unidentified transmembrane escorting proteins linking Shh to the cytosolic sorting machinery
384 or a default pathway from the basolateral cell surface.

385 Cholesterol modification is a crucial determinant in Hh protein membrane association,
386 mode of secretion and morphogenetic extension range (Callejo et al., 2011; Gallet et al., 2003;
387 Lewis et al., 2001; Porter et al., 1996). We find that Shh mutant lacking palmitoylation and
388 cholesterylation is secreted unpolarized. Therefore, the Shh peptidic structure either lacks
389 specific sorting signals for polarity or requires membrane association to expose sorting
390 competent proteinaceous signals. Our results also show that mutants lacking either
391 palmitoylation (ShhNpC24S) or cholesterylation (ShhN) predominantly distribute to the
392 basolateral cell surface, suggesting that both lipid modifications contribute to the basolateral
393 sorting of Shh. We could not attribute a particular role of palmitoylation in the basolateral-to-
394 apical trafficking because Shh defective in cholesterol modification is inefficiently palmitoylated
395 (Chen et al., 2004; Feng et al., 2004; Kohtz et al., 2001; Sbrogna et al., 2003). On the other
396 hand, our pulse chase and basolateral tagging experiments indicate that the cholesteryl group
397 can drive the entire polarized trafficking pathway of Shh, including the primary basolateral
398 sorting and subsequent transcytosis to the apical domain. It is possible that cholesterol
399 represents a sorting signal decoded at different steps of the Shh itinerary to the apical cell
400 surface, perhaps involving the trafficking role proposed for Disp (Callejo et al., 2011; D'Angelo
401 et al., 2015; Gore et al., 2021; Stewart et al., 2018), as a cholesterol binding protein (Cannac et
402 al., 2020; Chen et al., 2020).

403 Disp-1 is a multipass transmembrane protein with a luminal/extracellular sterol-sensing
404 domain that binds Shh in a cholesterol-dependent manner and is required for its release in a
405 diffusible form from the membrane (Burke et al., 1999; Cannac et al., 2020; Chen et al., 2020;
406 Creanga et al., 2012; Tukachinsky et al., 2012). In vertebrates, Disp-1 transfers Shh from the
407 cell surface to secreted SCUBE2 requiring the sodium gradient across the plasma membrane
408 (Burke et al., 1999; Cannac et al., 2020; Chen et al., 2020; Petrov et al., 2020). Stewart et al.
409 (Stewart et al., 2018) recently described that Disp-1 acquires functional competence after its

410 cleavage by the proprotein convertase furin at the cell surface (Stewart et al., 2018). Because
411 furin recycles between the TGN and the basolateral cell surface (Simmen et al., 1999), Disp-1
412 should reach first the basolateral cell surface to become competent in Hhs secretion in epithelial
413 cells (Stewart et al., 2018). In *Drosophila*, exogenously expressed Disp has been reported at
414 the plasma membrane of the apical, basal and lateral regions (D'Angelo et al., 2015), or mainly
415 at the basolateral plasma membrane (Callejo et al., 2011; Stewart et al., 2018). In MDCK cells,
416 transfection experiments showed Disp-1 distributed to the basolateral region seemingly due to
417 sorting information contained in its intracellular domain (Etheridge et al., 2010). We find with
418 RT-PCR that MDCK cells express Disp-1 (not shown) and our microinjection experiments
419 avoiding a saturating overexpression revealed recently synthesized Disp-1 predominantly
420 distributed at the subapical region, just underneath Shh, though also spreading throughout the
421 cell. These observations most likely reflect a dynamic Disp-1 trafficking and variations
422 depending on its expression levels and experimental conditions.

423 Our experiments of plasmid microinjection combined with live cell imaging show that
424 slightly overexpressed Disp-1 enhances basolateral secretion of newly expressed Shh just after
425 releasing a TGN block. Etheridge et al. (Etheridge et al., 2010) described a decreased
426 basolateral secretion of Shh under conditions of Disp-1 silencing or Disp-1 mutant expression in
427 MDCK cells. Accordingly, we find that coexpression of the cleavage defective Disp-CS mutant
428 (Stewart et al., 2018) decreases the basolateral secretion of Shh. A trade-off between apical
429 and basolateral Hh secretion has been previously proposed in the wing disk epithelia (Ayers et
430 al., 2010; Gore et al., 2021). Our results showing that basolateral secretion of Shh directly from
431 the TGN requires and can be enhanced by increasing the coexpressed level of Disp-1
432 suggesting that conditions that increase or decrease this process would determine how much
433 Hhs reaches the apical cell surface, where Disp is also expected to mediate Hhs secretion,
434 (D'Angelo et al., 2015).

435 Disp has been proposed to play a role in Hh subcellular distribution and trafficking
436 through endocytic pathways. This notion derives from studies in Drosophila epithelia models
437 where Hh secretion and signaling are sensitive to alterations in small GTPases such as Rab4,
438 Rab5, Rab8 and Rab11, which regulate endosomal compartments (Callejo et al., 2011;
439 D'Angelo et al., 2015; Gore et al., 2021; Pizette et al., 2021; Stewart et al., 2018). The
440 expression of Disp-1-CS previously suggested a requirement of Disp-1 cleavage in endosomal

441 membrane trafficking (Stewart et al., 2018). More recent evidence in *Drosophila* highlights a role
442 of Disp and Rab11 in Hh delivery from a tubular endosomal compartment named Hherisomes,
443 which modifies Hh signaling potential (Pizette et al., 2021). It is unknown whether this
444 compartment is functionally related to the Rab11-ARE compartment of MDCK cells (Perez Bay
445 et al., 2016). Our microinjection experiments show colocalization of newly synthesized Disp-1
446 and Shh together with Rab11 in a tubular subapical endosome corresponding to the ARE.
447 Furthermore, we show that Disp-1-CS not only decreases basolateral secretion from the TGN
448 but also accumulates Shh at the ARE, thus decreasing its apical cell surface distribution.
449 Therefore, our results add more evidence to support a role of Disp-1 in the vesicular trafficking
450 of Hhs, revealing a requirement for Shh trafficking along the basolateral-to-apical transcytosis
451 pathway at the level of the Rab11-ARE compartment.

452 The complex trafficking behavior of Shh in MDCK cells is compatible with the apical
453 and/or basolateral distribution and secretion of Hh seen in different epithelial cells, predicting
454 also a reciprocal basolateral versus apical secretion variations. In MDCK cells, the predominant
455 Shh apical location and secretion at steady state would result from low levels of Shh basolateral
456 secretion. Parietal cells in the stomach distribute and secrete Shh mostly apically, also showing
457 detectable levels at the basolateral side (Zavros et al., 2008). Basolateral secretion of Shh can
458 be inferred from stromal mesenchymal cell responses in intestinal cells (Buller et al., 2012;
459 Shyer et al., 2015) and kidney epithelium (Ding et al., 2012; Edeling et al., 2016; Zhou et al.,
460 2014), without discarding an apical secretion with other functions. Apical and basolateral
461 secretion of Shh sustaining distinct roles and signaling have been described in mature airway
462 epithelia (Mao et al., 2018). Here, immunostaining localizes Shh both at apical and lateral
463 regions and Shh basolateral release stimulates the stromal mesenchymal cells through primary
464 cilia, while its apical secretion induces non-canonical signaling via motile cilia (Mao et al., 2018).
465 In our proposed model the efficiency of Shh endocytic removal for transcytosis and/or secretion
466 from the basolateral domain would determine the relative distribution and secretion from each
467 domain.

468 Our results might also help to reconcile debated models in *Drosophila* epithelial
469 systems (Guerrero and Kornberg, 2014; Matusek et al., 2020). The relative magnitude of apical
470 and basolateral exocytic pathways operating in the long studied wing disc epithelia is unknown
471 (Guerrero and Kornberg, 2014; Matusek et al., 2020). Extensive studies in the wing disc

472 epithelia proposes a primary addressing of Hh towards the apical plasma membrane, even
473 though it is detected both in apical and basolateral cell surfaces (Callejo et al., 2011; D'Angelo
474 et al., 2015; Gradilla and Guerrero, 2013; Therond, 2012). A long controversy stands on
475 whether secretion for long-range Hh signaling occurs from the apical domain after endocytic
476 recycling (D'Angelo et al., 2015), or from the basolateral cell surface following apical-to-
477 basolateral transcytosis (Callejo et al., 2011). However, previous studies suggested a primary
478 Hh basolateral addressing followed by transcytosis to the apical domain instead, which might
479 explain the enhanced basolateral Hh distribution seen when Disp is silenced in other embryo
480 epithelial cells (Gallet et al., 2003). Basolateral Hh accumulation and secretion has also been
481 found under conditions that silenced the small GTPase Rab8, known to be involved in endocytic
482 and basolateral trafficking (Gore et al., 2021). These controversial views reflect the difficulties of
483 attributing a trafficking pathway based on the interpretation of locations and cell target
484 responses under steady-state conditions. As we show in MDCK cells, a predominant steady-
485 state apical cell surface distribution can result from a primary basolateral sorting from the TGN
486 followed by transcytosis. Our results also demonstrate that transcytosis of Shh still bound to the
487 membrane occurs not only from the basolateral but also from the apical domain. Although we
488 did not measure apical recycling after apical endocytosis, as described in the wing disk epithelia
489 (D'Angelo et al., 2015), this pathway might indeed operate together with transcytosis. Therefore,
490 our results are compatible with the observations in *Drosophila* epithelial systems and perhaps
491 can be used to reinterpret conflicting Hh trafficking models.

492 Hh proteins have been found secreted in different ways, including multimers (Gallet et
493 al., 2006; Zeng et al., 2001), lipoprotein particles (Panakova et al., 2005), extracellular vesicles
494 (Gradilla et al., 2014; Matusek et al., 2014; Parchure et al., 2015; Tanaka et al., 2005; Vyas et
495 al., 2014) and associated with cytonemes that are long filopodia (Bischoff et al., 2013; Chen et
496 al., 2017; Gonzalez-Mendez et al., 2017). How a primary basolateral sorting followed by
497 transcytosis relates with particular forms of Shh secretion remains a challenge for future
498 studies. Hh proteins form nano-scaled oligomers via electrostatic interactions and this process
499 is required for endocytosis followed by targeting to multivesicular bodies and secretion in
500 exosomes (Parchure et al., 2015; Vyas et al., 2008; Vyas et al., 2014). The role of this Shh
501 oligomerization in polarized sorting can now be evaluated in future experiments using the
502 proposed model in MDCK cells.

503 An indirect trafficking towards the apical cell surface includes several intermediate
504 stages where regulation might occur impacting upon Shh polarized secretion. This would allow
505 for reciprocal basolateral versus apical secretion variations in distinct epithelial contexts.
506 Conditions that increase basolateral secretion would decrease apical secretion. Variations in
507 Disp-1 expression will first impact the Shh basolateral secretion and then its transcytosis-
508 dependent apical secretion. This, together with the regulation of endocytic trafficking through
509 Rab GTPases, can contribute to determine variations in the basolateral versus apical secretion
510 and the signaling extension of this powerful regulatory molecule in morphogenesis and cancer.
511

512 **MATERIALS AND METHODS**

513 Experimental procedures

514

515 Key resources table

Reagent type (species) or resource	Designation	Source or reference	Identifiers	Additional information
Cell line (cannis familiaris)	MDCK (Madin-Darby canine kidney) II cells	ATCC provided by Enrique Rodriguez-Boulan (Weill Cornell Medical College, New York, NY)		
Culture media	DMEM	Thermo Fisher	12100046	
Culture media	DMEM methionine and cystine free	Thermo Fisher	21013024	for metabolic label
Culture media	DEMEM-HEPES	Thermo Fisher	12430054	for microinjection and live cell imaging
Transfected/ microinjected construct (M. musculus)	pCDNA3.1-Shh	This paper		Subcloned from pBluescript-mShh (P. A. Beachy) (Development 1994)
Transfected construct (M. musculus)	pCDNA3.1-ShhNC24S	This paper		Subcloned from pRK5-mShhNC24S (P. A. Beachy) (J Cell Sci 1999)
Transfected construct (M. musculus)	pCDNA3.1-ShhN	This paper		PCR cloning from pCDNA3.1-Shh
Transfected construct (M. musculus)	pCDNA3.1-ShhNpC24S	This paper		Subcloned from pSK-C24S (P. A. Beachy)
Microinjected construct (M. musculus)	pCDNA3-Shh-GFP	McMahon Lab (Chamberlain 2008)		
Cell line (cannis familiaris)	MDCK-Rab11-mCherry	This paper		Stably expressing human Rab11a-mCherry
Cell line (cannis familiaris)	MDCK-GFP-NO-GPI	Imjeti 2011		Stably expressing GFP-NO-GPI
Microinjected construct (M. musculus)	pCDNA3 V5-Dispatched-HA	Ogden Lab (Stewart 2018)		pCDNA3 from Invitrogen
Microinjected construct (M. musculus)	pCDNA3 V5-Dispatched-CS-HA	Ogden Lab (Stewart 2018)		pCDNA3 from Invitrogen
Microinjected construct (M. musculus)	LDLR-GFP-Y18A	Matter 1992		(pCB6, Hunziker 1991) LDLR-GFP-Y18A
Antibody	Anti-Shh	DSHB (Developmental Studies Hybridoma Bank)	5E1	IF (1:50) IP (1:50)
Antibody	Anti-Shh	Santa Cruz Biotechnology, Inc. (California, USA)	sc-9024 (H-160)	WB (1:1000)
Antibody	Anti-E-cadherin	Cell signaling	24E10 mAb #3195	IF (1:100)
Antibody	Anti-E-cadherin	BD transduction		IP (2mg/sample)

		laboratories		
Antibody	Anti-GFP (rabbit)	This paper		IP (1:250)
Antibody	Anti-Rab11a (rabbit)	Thermo Fisher Scientific	715300	IF (1:100)
Antibody	Anti-Fibronectin	Sigma	F6140	WB (1:2000)
Antibody	Anti-Na^+/K^+-ATPase	Santa Cruz Biotechnology, Inc. (California, USA)	sc-21713	WB (1:2000)
Antibody	Anti-HA (chicken)	Millipore	AB3254	IF (1:100)
Antibody	AlexaFluor 488	Life technologies, Carlsbad, CA	A11029 (Mouse) A11034 (Rabbit) A-11039 (Chicken)	1:500
Antibody	AlexaFluor 555	Life technologies	A21424 (Mouse) A21429 (Rabbit) A32932 (Chicken)	1:500
Antibody	AlexaFluor 647	Life technologies	A21235 (Mouse)	1:500
Fluorescent dye	Hoechst	Thermo Fisher Scientific	62249	1:1000
Software, algorithm	Adobe Photoshop CS4	Adobe, San Jose, CA		for making figures
Software, algorithm	LAS X	Leica, Wetzlar, Germany		image analysis
Software, algorithm	Prism	GraphPad, La Jolla, CA		for statistical, analysis and graphs
Software, algorithm	SigmaPlot10 software			for quantification of golgi retention
Software, algorithm	Huygens Professional software			for deconvolution images
Software, algorithm	ImageJ (NIH)		2.0.0-rc-69/1.52o	image analysis
Software, algorithm	OptiQuant software	PerkinElmer	3.0	
Commercial assay or kit	Lipofectamine 2000	Thermo Fisher Scientific	11668027	
Commercial assay or kit	Pierce™ ECL Western Blotting Substrate	Pierce™, Waltham, MA, USA	32106	
Chemical compound, drug	Sulfo-NHS-LC-biotin	Pierce™ /Thermo Fisher Scientific	21335	
Chemical compound, drug	EZ-Link™ NHS-SS-Biotin	Pierce/Thermo Fisher Scientific	21441	
Chemical compound, drug	NeutrAvidin-agarose	Pierce/Thermo Fisher Scientific	29201	
Chemical compound, drug	MesNa	Sigma	PHR1570	
Chemical compound, drug	^{35}S-methionine/cysteine	Perkin Elmer NEN Life Science Products (Boston, USA)	NEG709A005MC	
Chemical compound, drug	Fluoromount-G	Thermo Fisher Scientific	00495802	
Polarized culture	24mm Transwells	Costar	3412	for biochemistry

chamber				
Polarized culture chamber	12mm Transwells	Costar	3401	for immunofluorescence

516
517 Cloning and Subcloning
518 cDNA coding for Shh (from pBlueScript-Shh), ShhNpC24S (from pSK-C24S) and
519 ShhNC24S (from pRK5-ShhNC24S) (kindly provided by Philip A. Beachy, Stanford University,
520 CA, USA) were subcloned by double digestion with EcoRI and XbaI (for Shh), NotI (for
521 ShhNpC24S) or NotI and KpnI (for ShhNC24S) restriction enzymes and ligated into pcDNA3.1(-
522) with T4 DNA ligase (Thermo Fisher cat #15224017) according to the manufacturer's
523 instructions. ShhN dsDNA coding for residues 1-198 of murine Shh was obtained by PCR using
524 Pfu polymerase (Promega cat # M7741) and the following primers: Fw:
525 GTCTCGAGCCAACTCCGATGTGTTCCG and Rev: CGGAATTCTTAGCCGCCGGATTTGGCC
526 that include XhoI and EcoRI sites for subcloning into pcDNA3.1(+). All constructs were
527 confirmed by sequencing.
528
529 Cell Lines
530 MDCK cells were grown in DMEM (Cat# 12100046, Thermo Fisher) supplemented with
531 7.5% fetal bovine serum (FBS, Cat# SH30071.03 HyClone), 50 U/mL antibiotics (Penicillin-
532 Streptomycin mix (Cat# 15070063, Thermo Fisher), and 5 µg/ml Plasmocin (Cat# ant-mpp,
533 InvivoGen), in a 37ºC, 5% CO_2 humidified incubator, routinely analyzed by RT-PCR for
534 mycoplasma contamination. Passages were made before reaching confluence every 2-3 days
535 by two washes with PBS (15 min each) and incubation in trypsin 0.05% for 5-10 min (Trypsin
536 Cat#15400054, Thermo Fisher). MDCK cells stable transfected clones (MDCK-Shh, -ShhN, -
537 ShhNC24S, -ShhNpC24S) were generated by transfection with Lipofectamine 2000 reagent and
538 selection by G418 resistance.
539
540 Transfection
541 MDCK (100.000 cells) grown in 24-multiwell plates were transfected with 1µg of plasmid
542 DNA and Lipofectamine 2000 reagent, trypsinized the next day and plated at 1/10 and 1/100
543 dilution into 100mm dishes. Selection media containing G418 (0.8mg/ml) was added the next
544 day, changed every 5 days until visible colonies were isolated using cloning cylinders and
545 expanded in 6-multiwell plates. Screening was made by immunofluorescence (see below) and
546 immunoblot of lysates and media (See “Protein Analysis”).
547
548 Cell lysates and protein analysis
549 To obtain lysates cells were washed twice in PBS containing 1 mM MgCl2, 0.1mM
550 CaCl2 (PBS-CM) and lysed in 500 µl RIPA buffer (50 mM Tris-HCl (pH 8.0), 150 mM NaCl,
551 0.5% Na-deoxycholate, 0.1% SDS, 1% Triton X-100) supplemented with protease inhibitors
552 (PMSF 2mM, Leupeptin 2µg/ml, Pepstatin 1µg/ml). Recovered lysates were cleared by

553 centrifugation at 14.000rpm at 4ºC. Protein concentration was determined on the cleared cell
554 lysates with BCA method and 500 µg total protein was used for immunoprecipitation or
555 NeutrAvidin-precipitation (see below), 10% volume of each lysate was used as loading control.
556
557 Steady-state Shh Secretion
558 Analysis of secreted proteins was performed by collection of conditioned media in low
559 serum media (0.3% FBS), precipitation in 10% trichloroacetic acid (TCA) and incubation for
560 30min on ice. Precipitated proteins were centrifuged at 4ºC and 14.000 rpm for 10 min, washed
561 once with 1ml of 100% acetone and re-centrifuged. Pellets were solubilized in 30µl of NaOH
562 0.1M and 10µl of 3X Laemmli sample buffer. Lysates and/or secreted proteins were resolved in
563 12%SDS-PAGE, transferred to PVDF membranes and immunoblotted with the indicated
564 antibodies.
565
566 Polarized monolayers of MDCK cells grown in Transwell inserts
567 MDCK cells (100,000-400,000 cells) were plated on 12 mm or 24-mm Transwell inserts,
568 0.4-mm pore size (Costar), and grown with daily media changes until the
569 transepithelial resistance reached 400 ohm/cm^2 (4–5 days) measured with an EVOM
570 electrometer (World Precision Instruments, Sarasota, FL).
571
572 Immunofluorescence
573 Cells were fixed in freshly prepared 4% PFA in PBS-CM for 15 min at room temperature
574 or overnight at 4°C. To analyze subcellular distribution of interest proteins, cells were
575 permeabilized with 0.2% saponin in PBS-CM. All subsequent steps contained 0.2% saponin.
576 Primary and secondary antibodies were incubated for 30 min at 37°C or overnight at 4°C.
577 Coverslips were mounted in Fluoromount.
578
579 Protein immunoprecipitation
580 The key resources table indicates the amount of antibodies (GFP, E-cadherin, 5E1)
581 used per sample. Antibodies were pre-incubated with 30µl of protein-A sepharose for 2h at 4°C,
582 then beads were washed 3 times to remove excess antibodies. Total cell lysate (approx. 500
583 µg) or collected medium was then added to beads and incubated for 2h at 4ºC, washed 3 times
584 in RIPA buffer and eluted in 30µl of 2X Laemmli Buffer.
585
586 Domain-Selective Surface Biotinylation
587 Steady-state apical and basolateral distribution of Shh and endogenous proteins were
588 analyzed by domain selective biotinylation of MDCK cells grown in Transwell inserts, as
589 described (Bravo-Zehnder et al., 2000; Oyanadel et al., 2018). Cells were rinsed twice with ice-
590 cold PBS-CM followed by two successive 20 min incubations at 4ºC with 0.5 mg/ml Sulfo-NHS-

591 LC-Biotin in PBS-CM, added to the apical (0.6 ml) or basolateral (1 ml) sides. Cells were then
592 incubated with 50mM NH_4Cl in PBS-CM for 10 min, rinsed twice with PBS-CM and lysed in
593 RIPA buffer, supplemented with proteases inhibitors for 30 min at 4ºC. NeutrAvidin-Sepharose
594 was used to retrieve biotinylated proteins by centrifugation (18,000 x g for 10 min), which then
595 were analyzed by immunoblot against Shh and endogenous proteins, as described (Bravo-
596 Zehnder et al., 2000; Oyanadel et al., 2018; Sargiacomo et al., 1989).
597
598 Pulse-chase domain-selective targeting of newly synthesized proteins
599 Biotinylation targeting assay was used to assess biosynthetic delivery of proteins to
600 apical and basolateral PM domains. Stable transfected cells were pulse-labeled in methionine-
601 free and cysteine-free DMEM supplemented with 400 µCi/ml [^{35}S]-methionine/cysteine for 30
602 min in 120µl of medium applied to the basolateral side of the inverted filter, as described
603 (Marzolo et al., 1997). Chase was made for different times in culture media containing 300 µM
604 cycloheximide (CHX) and 3- to 6-fold excess cold methionine (0.6mM) and cysteine and
605 (1.2mM). Cells were then subjected to domain-selective surface biotinylation, chilled in ice-cold
606 PBS-CM and lysed with RIPA buffer supplemented with protease inhibitors at 4ºC for 30 min.
607 Lysates were cleared by centrifugation (18,000 x g for 10 min) before immunoprecipitation with
608 protein-A-Sepharose preincubated antibodies (5E1-anti-Shh or E-cadherin). The mixture of
609 biotinylated (surface) plus non-biotinylated (intracellular) immunoprecipitated proteins was
610 incubated at 95º for 5 min in 30 µl of 10% SDS RIPA to dissociate immune complexes. The
611 eluted proteins were diluted to 1 ml with RIPA and subjected to NeutrAvidin-Sepharose
612 precipitation to isolate surface-located Shh. In addition, secreted Shh was immunoprecipitated
613 from the apical and basolateral media with protein-A-Sepharose bound 5E1, as described for
614 other proteins (Gonzalez et al., 1993; Gonzalez et al., 1987; Marzolo et al., 1997). The immune
615 complexes of surface-located and secreted Shh were resolved by SDS-PAGE. [^{35}S]-
616 methionine/cysteine labeled proteins were visualized in fluorograms made with Amplify^{TM}
617 fluorography reagent (Amersham), developed in scanner Cyclone Plus (Perkin Elmer) with
618 OptiQuant software (3.0, Perkin Elmer).
619
620 Transcytosis assays
621 Trafficking of Shh from one cell surface domain to the opposite (transcytosis) was
622 analyzed by domain-specific biotinylation and cell surface-tagging immunofluorescence assays.
623 *1. Biotinylation transcytosis assay* was performed with reducible biotin reagent Sulfo-
624 NHS-SS-biotin as described (Burgos et al., 2004). In brief, six Transwell filter cups with
625 polarized live MDCK monolayer cells were subjected to basolateral-specific biotinylation with
626 Sulfo-NHS-SS-biotin in *PBS-CM.* One filtercup was used for total basolateral biotinylated Shh
627 ("non-reduced, time 0"), and other two filtercups were subjected to either apical or basolateral
628 reduction with 22 mM MesNa reagent (0 min) made in buffer 50 mM Tris-HCl, pH 8.6, 100 mM

629 NaCl. The remaining three filtercups were incubated for 120 min in 37ºC in growth media to
630 allow trafficking and then MesNa was added to the apical or basolateral side. Monolayers were
631 alkylated with 20mM iodoacetamide in PBS-CM containing 1%BSA, washed twice in PBS-CM,
632 lysed in Ripa Buffer supplemented with protease inhibitors and subjected to NeutrAvidin-
633 Sepharose precipitation and immunoblot. To analyze apical secretion of Shh present in the
634 basolateral membrane, cells were biotinylated from the basolateral side and then incubated in
635 DMEM, 0.5 % fetal bovine serum at 37ºC for 2 hours. Biotinylated Shh proteins were retrieved
636 from apical and basolateral media with NeutrAvidin-Sepharose and immunoblotted.
637 *2. Cell surface-tagging immunofluorescence transcytosis assay.* Live MDCK cells
638 grown in Transwell inserts were apically or basolaterally incubated with 5E1 antibody diluted in
639 DMEM (supplemented with 10mM HEPES) for 30 min at 4°C. After 3 washes in PBS-CM, cells
640 were shifted to 37°C in growth media to allow trafficking for different times, fixed at different
641 times with PFA-PBS-CM and permeabilized. Shh bound to the primary antibody was detected
642 by incubation of fluorophore-coupled secondary antibodies for 30 min at 37°C.
643 *3. Secretion of basolaterally-sorted ShhNpC24S.* MDCK cells grown in Transwell
644 inserts were rinsed twice with ice-cold PBS-CM followed by two successive 20 min incubations
645 at 4ºC with 0.5 mg/ml Sulfo-NHS-LC-Biotin in PBS-CM, added to the basolateral sides. Cells
646 were then incubated with 50mM NH_4Cl in PBS-CM for 5 min, rinsed twice with PBS-CM and
647 shifted to 37°C in growth media for 2h. Then apical and basolateral media was collected and
648 precipitated with Neutravidin (basolaterally-biotinylated secreted proteins). Samples were
649 analyzed by western blot.
650
651 Microinjection
652 MDCK cells were plated either in 12mm diameter glass coverslips (5000 cells) the
653 absence of Plasmocin. After achieving full confluence (4-5 cells) microinjections were performed
654 in the cell nucleus (plasmids) using back-loaded glass capillaries, an Eppendorf NI2
655 micromanipulator and an Eppendorf Transjector 5246 system. The expression plasmids DNAs
656 were used at a concentration of 20 to 100ng/µl in buffer HEPES 10 mM pH7.4, KCl 140 mM.
657 During the microinjection procedure cells were maintained in DMEM-HEPES.
658
659 Live cell imaging
660 The microinjection approach to express and accumulate exogenous proteins at the
661 TGN and then assess subsequent trafficking was performed as described (Cancino et al., 2007;
662 Kreitzer et al., 2000). Briefly, microinjected cells were incubated for 45 min at 37°C in DMEM-
663 HEPES plus 7.5% FSB to allow protein expression without ER leakage, plasmid concentration
664 was adjusted (20 to 100ng/µl) to obtain enough protein expression to be detected by
665 fluorescence microscopy and then the exocytic trafficking was arrested at the TGN by

incubating the cells at 20°C for 2 h in DMEM-HEPES with CHX. After the 20°C block the cells were mounted on a Leica SP8 microscope in DMEM-HEPES plus CXM and incubated at 37°C.

Images acquisition and processing

Images were collected at 1024 × 1024 resolution in Z stacks of 300-nm steps using a Leica SP8 confocal microscope and a 63× oil immersion 1.4 ma lens, and processed with ImageJ free software, NIH. High Resolution images were acquired at Nyquist rate parameters (Nyquist Calculator, SVI, NL) and the resulting oversampled images were deconvoluted with Huygens Essential Software (SVI, NL), which was also used for 3D surface rendering processing.

Statistical Analysis

Significance was determined with Prism software using Student's t-test. For all statistical analyses **$p<0.05$ and ****$p<0.0001$. Error bars indicate standard error of mean (SEM).

ACKNOWLEDGEMENTS

We are grateful to Dr. Stacey Ogden (St. Jude Children's Research Hospital, USA) for kindly providing Dispatched plasmids constructs, Dr. Andrew P. McMahon (University of Southern California, USA) and Dr. Philip A. Beachy (Stanford University School of Medicine, USA) for kindly providing Shh plasmids constructs.

ADDITIONAL INFORMATION

Funding

Funder	Grant reference number	Author
Fondo Nacional de Desarrollo Científico y Tecnológico (FONDECYT)	1181907	Alfonso González
Programa de Apoyo a Centros con Financiamiento Basal. Agencia Nacional de Investigación y Desarrollo (ANID)	#AFB170004; #AFB170005; #ACE210009	Alfonso González
Postdoctoral Project (FONDECYT)	3150603	Lisette Sandoval

AUTHOR CONTRIBUTIONS

Lisette Sandoval, Conceptualization, Data curation, Formal analysis, Validation, Investigation, Visualization, Methodology, Writing - original draft, Writing - review and editing; Mariana Labarca, Conceptualization, Formal analysis, Validation, Investigation, Visualization, Methodology, Writing - review and editing; Claudio Retamal, Data curation, Formal analysis, Methodology; Juan Larraín, Conceptualization, Resources; Alfonso González, Conceptualization, Supervision, Funding acquisition, Writing

699 **REFERENCES**

700 Apodaca, G., Katz, L.A., and Mostov, K.E. (1994). Receptor-mediated transcytosis of IgA in MDCK cells is
701 via apical recycling endosomes. J Cell Biol *125*, 67-86.

702 Arkhipenko, A., Syan, S., Victoria, G.S., Lebreton, S., and Zurzolo, C. (2016). PrPC Undergoes Basal to
703 Apical Transcytosis in Polarized Epithelial MDCK Cells. PLoS One *11*, e0157991.

704 Ayers, K.L., Gallet, A., Staccini-Lavenant, L., and Therond, P.P. (2010). The long-range activity of
705 Hedgehog is regulated in the apical extracellular space by the glypican Dally and the hydrolase Notum.
706 Developmental cell *18*, 605-620.

707 Bartles, J.R., Feracci, H.M., Stieger, B., and Hubbard, A.L. (1987). Biogenesis of the rat hepatocyte
708 plasma membrane in vivo: comparison of the pathways taken by apical and basolateral proteins using
709 subcellular fractionation. J Cell Biol *105*, 1241-1251.

710 Beachy, P.A., Karhadkar, S.S., and Berman, D.M. (2004). Tissue repair and stem cell renewal in
711 carcinogenesis. Nature *432*, 324-331.

712 Bischoff, M., Gradilla, A.C., Seijo, I., Andres, G., Rodriguez-Navas, C., Gonzalez-Mendez, L., and
713 Guerrero, I. (2013). Cytonemes are required for the establishment of a normal Hedgehog morphogen
714 gradient in Drosophila epithelia. Nat Cell Biol *15*, 1269-1281.

715 Bonifacino, J.S. (2014). Adaptor proteins involved in polarized sorting. J Cell Biol *204*, 7-17.

716 Bravo-Zehnder, M., Orio, P., Norambuena, A., Wallner, M., Meera, P., Toro, L., Latorre, R., and Gonzalez,
717 A. (2000). Apical sorting of a voltage- and Ca2+-activated K+ channel alpha -subunit in Madin-Darby
718 canine kidney cells is independent of N-glycosylation. Proc Natl Acad Sci U S A *97*, 13114-13119.

719 Briscoe, J., and Therond, P.P. (2013). The mechanisms of Hedgehog signalling and its roles in
720 development and disease. Nature reviews Molecular cell biology *14*, 416-429.

721 Brown, P.S., Wang, E., Aroeti, B., Chapin, S.J., Mostov, K.E., and Dunn, K.W. (2000). Definition of distinct
722 compartments in polarized Madin-Darby canine kidney (MDCK) cells for membrane-volume sorting,
723 polarized sorting and apical recycling. Traffic *1*, 124-140.

724 Buller, N.V., Rosekrans, S.L., Westerlund, J., and van den Brink, G.R. (2012). Hedgehog signaling and
725 maintenance of homeostasis in the intestinal epithelium. Physiology (Bethesda) *27*, 148-155.

726 Burgos, P.V., Klattenhoff, C., de la Fuente, E., Rigotti, A., and Gonzalez, A. (2004). Cholesterol depletion
727 induces PKA-mediated basolateral-to-apical transcytosis of the scavenger receptor class B type I in MDCK
728 cells. Proc Natl Acad Sci U S A *101*, 3845-3850.

729 Burke, R., Nellen, D., Bellotto, M., Hafen, E., Senti, K.A., Dickson, B.J., and Basler, K. (1999). Dispatched,
730 a novel sterol-sensing domain protein dedicated to the release of cholesterol-modified hedgehog from
731 signaling cells. Cell *99*, 803-815.

732 Callejo, A., Bilioni, A., Mollica, E., Gorfinkiel, N., Andres, G., Ibanez, C., Torroja, C., Doglio, L., Sierra, J.,
733 and Guerrero, I. (2011). Dispatched mediates Hedgehog basolateral release to form the long-range
734 morphogenetic gradient in the Drosophila wing disk epithelium. Proc Natl Acad Sci U S A *108*, 12591-
735 12598.

736 Cancino, J., Torrealba, C., Soza, A., Yuseff, M.I., Gravotta, D., Henklein, P., Rodriguez-Boulan, E., and
737 Gonzalez, A. (2007). Antibody to AP1B adaptor blocks biosynthetic and recycling routes of basolateral
738 proteins at recycling endosomes. Mol Biol Cell *18*, 4872-4884.

739 Cannac, F., Qi, C., Falschlunger, J., Hausmann, G., Basler, K., and Korkhov, V.M. (2020). Cryo-EM
740 structure of the Hedgehog release protein Dispatched. Sci Adv *6*, eaay7928.

741 Caspary, T., Garcia-Garcia, M.J., Huangfu, D., Eggenschwiler, J.T., Wyler, M.R., Rakeman, A.S., Alcorn,
742 H.L., and Anderson, K.V. (2002). Mouse Dispatched homolog1 is required for long-range, but not
743 juxtacrine, Hh signaling. Curr Biol *12*, 1628-1632.

744 Chamberlain, C.E., Jeong, J., Guo, C., Allen, B.L., and McMahon, A.P. (2008). Notochord-derived Shh
745 concentrates in close association with the apically positioned basal body in neural target cells and forms a
746 dynamic gradient during neural patterning. Development *135*, 1097-1106.

747 Chen, H., Liu, Y., and Li, X. (2020). Structure of human Dispatched-1 provides insights into Hedgehog
748 ligand biogenesis. Life Sci Alliance *3*.

749 Chen, M.H., Li, Y.J., Kawakami, T., Xu, S.M., and Chuang, P.T. (2004). Palmitoylation is required for the
750 production of a soluble multimeric Hedgehog protein complex and long-range signaling in vertebrates.
751 Genes Dev *18*, 641-659.

752 Chen, W., Huang, H., Hatori, R., and Kornberg, T.B. (2017). Essential basal cytonemes take up Hedgehog
753 in the Drosophila wing imaginal disc. Development *144*, 3134-3144.

754 Chen, X., Tukachinsky, H., Huang, C.H., Jao, C., Chu, Y.R., Tang, H.Y., Mueller, B., Schulman, S.,
755 Rapoport, T.A., and Salic, A. (2011). Processing and turnover of the Hedgehog protein in the endoplasmic
756 reticulum. J Cell Biol *192*, 825-838.

757 Creanga, A., Glenn, T.D., Mann, R.K., Saunders, A.M., Talbot, W.S., and Beachy, P.A. (2012). Scube/You
758 activity mediates release of dually lipid-modified Hedgehog signal in soluble form. Genes Dev *26*, 1312-
759 1325.

760 D'Angelo, G., Matusek, T., Pizette, S., and Therond, P.P. (2015). Endocytosis of Hedgehog through
761 dispatched regulates long-range signaling. Developmental cell *32*, 290-303.

762 Danesin, C., Agius, E., Escalas, N., Ai, X., Emerson, C., Cochard, P., and Soula, C. (2006). Ventral neural
763 progenitors switch toward an oligodendroglial fate in response to increased Sonic hedgehog (Shh) activity:
764 involvement of Sulfatase 1 in modulating Shh signaling in the ventral spinal cord. J Neurosci *26*, 5037-
765 5048.

766 Ding, H., Zhou, D., Hao, S., Zhou, L., He, W., Nie, J., Hou, F.F., and Liu, Y. (2012). Sonic hedgehog
767 signaling mediates epithelial-mesenchymal communication and promotes renal fibrosis. J Am Soc Nephrol
768 *23*, 801-813.

769 Edeling, M., Ragi, G., Huang, S., Pavenstadt, H., and Susztak, K. (2016). Developmental signalling
770 pathways in renal fibrosis: the roles of Notch, Wnt and Hedgehog. Nat Rev Nephrol *12*, 426-439.

771 Etheridge, L.A., Crawford, T.Q., Zhang, S., and Roelink, H. (2010). Evidence for a role of vertebrate Disp1
772 in long-range Shh signaling. Development *137*, 133-140.

773 Feng, J., White, B., Tyurina, O.V., Guner, B., Larson, T., Lee, H.Y., Karlstrom, R.O., and Kohtz, J.D.
774 (2004). Synergistic and antagonistic roles of the Sonic hedgehog N- and C-terminal lipids. Development
775 *131*, 4357-4370.

776 Gallet, A. (2011). Hedgehog morphogen: from secretion to reception. Trends Cell Biol *21*, 238-246.

777 Gallet, A., Rodriguez, R., Ruel, L., and Therond, P.P. (2003). Cholesterol modification of hedgehog is
778 required for trafficking and movement, revealing an asymmetric cellular response to hedgehog.
779 Developmental cell *4*, 191-204.

780 Gallet, A., Ruel, L., Staccini-Lavenant, L., and Therond, P.P. (2006). Cholesterol modification is necessary
781 for controlled planar long-range activity of Hedgehog in Drosophila epithelia. Development *133*, 407-418.

782 Gan, Y., McGraw, T.E., and Rodriguez-Boulan, E. (2002). The epithelial-specific adaptor AP1B mediates
783 post-endocytic recycling to the basolateral membrane. Nat Cell Biol *4*, 605-609.

784 Gonzalez, A., Nicovani, S., and Juica, F. (1993). Apical secretion of hepatitis B surface antigen from
785 transfected Madin- Darby canine kidney cells. J Biol Chem *268*, 6662-6667.

786 Gonzalez, A., Rizzolo, L., Rindler, M., Adesnik, M., Sabatini, D.D., and Gottlieb, T. (1987). Nonpolarized
787 secretion of truncated forms of the influenza hemagglutinin and the vesicular stomatitus virus G protein
788 from MDCK cells. Proc Natl Acad Sci U S A *84*, 3738-3742.

789 Gonzalez, A., and Rodriguez-Boulan, E. (2009). Clathrin and AP1B: key roles in basolateral trafficking
790 through trans-endosomal routes. FEBS Lett *583*, 3784-3795.

791 Gonzalez-Mendez, L., Seijo-Barandiaran, I., and Guerrero, I. (2017). Cytoneme-mediated cell-cell contacts
792 for Hedgehog reception. Elife *6*.

793 Gore, T., Matusek, T., D'Angelo, G., Giordano, C., Tognacci, T., Lavenant-Staccini, L., Rabouille, C., and
794 Therond, P.P. (2021). The GTPase Rab8 differentially controls the long- and short-range activity of the
795 Hedgehog morphogen gradient by regulating Hedgehog apico-basal distribution. Development *148*.

796 Gottlieb, T.A., Beaudry, G., Rizzolo, L., Colman, A., Rindler, M., Adesnik, M., and Sabatini, D.D. (1986).
797 Secretion of endogenous and exogenous proteins from polarized MDCK cell monolayers. Proc Natl Acad
798 Sci U S A *83*, 2100-2104.

799 Gradilla, A.C., Gonzalez, E., Seijo, I., Andres, G., Bischoff, M., Gonzalez-Mendez, L., Sanchez, V., Callejo,
800 A., Ibanez, C., Guerra, M.*, et al.* (2014). Exosomes as Hedgehog carriers in cytoneme-mediated transport
801 and secretion. Nature communications *5*, 5649.

802 Gradilla, A.C., and Guerrero, I. (2013). Hedgehog on the move: a precise spatial control of Hedgehog
803 dispersion shapes the gradient. Curr Opin Genet Dev *23*, 363-373.

804 Gravotta, D., Deora, A., Perret, E., Oyanadel, C., Soza, A., Schreiner, R., Gonzalez, A., and Rodriguez-
805 Boulan, E. (2007). AP1B sorts basolateral proteins in recycling and biosynthetic routes of MDCK cells.
806 Proc Natl Acad Sci U S A *104*, 1564-1569.

807 Guerrero, I., and Kornberg, T.B. (2014). Hedgehog and its circuitous journey from producing to target cells.
808 Seminars in cell & developmental biology *33*, 52-62.

809 Guo, X., Mattera, R., Ren, X., Chen, Y., Retamal, C., Gonzalez, A., and Bonifacino, J.S. (2013). The
810 adaptor protein-1 mu1B subunit expands the repertoire of basolateral sorting signal recognition in epithelial
811 cells. Developmental cell *27*, 353-366.

812 Hall, E.T., Cleverdon, E.R., and Ogden, S.K. (2019). Dispatching Sonic Hedgehog: Molecular Mechanisms
813 Controlling Deployment. Trends Cell Biol *29*, 385-395.

814 Hauri, H.P., and Matter, K. (1991). Protein traffic in intestinal epithelial cells. Semin Cell Biol *2*, 355-364.

815 Hua, W., Sheff, D., Toomre, D., and Mellman, I. (2006). Vectorial insertion of apical and basolateral
816 membrane proteins in polarized epithelial cells revealed by quantitative 3D live cell imaging. J Cell Biol
817 *172*, 1035-1044.

818 Hubbard, A.L. (1989). Endocytosis. Curr Opin Cell Biol *1*, 675-683.

819 Imjeti, N.S., Lebreton, S., Paladino, S., de la Fuente, E., Gonzalez, A., and Zurzolo, C. (2011). N-
820 Glycosylation instead of cholesterol mediates oligomerization and apical sorting of GPI-APs in FRT cells.
821 Mol Biol Cell *22*, 4621-4634.

822 Kohtz, J.D., Lee, H.Y., Gaiano, N., Segal, J., Ng, E., Larson, T., Baker, D.P., Garber, E.A., Williams, K.P.,
823 and Fishell, G. (2001). N-terminal fatty-acylation of sonic hedgehog enhances the induction of rodent
824 ventral forebrain neurons. Development *128*, 2351-2363.

825 Kreitzer, G., Marmorstein, A., Okamoto, P., Vallee, R., and Rodriguez-Boulan, E. (2000). Kinesin and
826 dynamin are required for post-Golgi transport of a plasma- membrane protein. Nat Cell Biol *2*, 125-127.

827 Kreitzer, G., Schmoranzer, J., Low, S.H., Li, X., Gan, Y., Weimbs, T., Simon, S.M., and Rodriguez-Boulan,
828 E. (2003). Three-dimensional analysis of post-Golgi carrier exocytosis in epithelial cells. Nat Cell Biol *5*,
829 126-136.

830 Le Bivic, A., Real, F.X., and Rodriguez-Boulan, E. (1989). Vectorial targeting of apical and basolateral
831 plasma membrane proteins in a human adenocarcinoma epithelial cell line. Proc Natl Acad Sci U S A *86*,
832 9313-9317.

833 Lebreton, S., Paladino, S., Liu, D., Nitti, M., von Blume, J., Pinton, P., and Zurzolo, C. (2021). Calcium
834 levels in the Golgi complex regulate clustering and apical sorting of GPI-APs in polarized epithelial cells.
835 Proc Natl Acad Sci U S A *118*.

836 Lebreton, S., Paladino, S., and Zurzolo, C. (2019). Clustering in the Golgi apparatus governs sorting and
837 function of GPI-APs in polarized epithelial cells. FEBS Lett *593*, 2351-2365.

838 Lehmann, G.L., Hanke-Gogokhia, C., Hu, Y., Bareja, R., Salfati, Z., Ginsberg, M., Nolan, D.J., Mendez-
839 Huergo, S.P., Dalotto-Moreno, T., Wojcinski, A.*, et al.* (2020). Single-cell profiling reveals an endothelium-
840 mediated immunomodulatory pathway in the eye choroid. J Exp Med *217*.

841 Lewis, P.M., Dunn, M.P., McMahon, J.A., Logan, M., Martin, J.F., St-Jacques, B., and McMahon, A.P.
842 (2001). Cholesterol modification of sonic hedgehog is required for long-range signaling activity and
843 effective modulation of signaling by Ptc1. Cell *105*, 599-612.

844 Lisanti, M.P., Sargiacomo, M., Graeve, L., Saltiel, A.R., and Rodriguez-Boulan, E. (1988). Polarized apical
845 distribution of glycosyl-phosphatidylinositol-anchored proteins in a renal epithelial cell line. Proc Natl Acad
846 Sci U S A *85*, 9557-9561.

847 Long, J., Tokhunts, R., Old, W.M., Houel, S., Rodgriguez-Blanco, J., Singh, S., Schilling, N., Capobianco,
848 A.J., Ahn, N.G., and Robbins, D.J. (2015). Identification of a family of fatty-acid-speciated sonic hedgehog
849 proteins, whose members display differential biological properties. Cell Rep *10*, 1280-1287.

850 Luton, F., Hexham, M.J., Zhang, M., and Mostov, K.E. (2009). Identification of a cytoplasmic signal for
851 apical transcytosis. Traffic *10*, 1128-1142.

852 Machado, M.V., and Diehl, A.M. (2017). Hedgehog signalling in liver pathophysiology. J Hepatol.

853 Mao, S., Shah, A.S., Moninger, T.O., Ostedgaard, L.S., Lu, L., Tang, X.X., Thornell, I.M., Reznikov, L.R.,
854 Ernst, S.E., Karp, P.H.*, et al.* (2018). Motile cilia of human airway epithelia contain hedgehog signaling
855 components that mediate noncanonical hedgehog signaling. Proc Natl Acad Sci U S A *115*, 1370-1375.

856 Marzolo, M.P., Bull, P., and Gonzalez, A. (1997). Apical sorting of hepatitis B surface antigen (HBsAg) is
857 independent of N-glycosylation and glycosylphosphatidylinositol-anchored protein segregation. Proc Natl
858 Acad Sci U S A *94*, 1834-1839.

859 Matusek, T., Marcetteau, J., and Therond, P.P. (2020). Functions of Wnt and Hedgehog-containing
860 extracellular vesicles in development and disease. J Cell Sci *133*.

861 Matusek, T., Wendler, F., Poles, S., Pizette, S., D'Angelo, G., Furthauer, M., and Therond, P.P. (2014).
862 The ESCRT machinery regulates the secretion and long-range activity of Hedgehog. Nature *516*, 99-103.

863 Mayor, S., and Riezman, H. (2004). Sorting GPI-anchored proteins. Nature reviews Molecular cell biology
864 *5*, 110-120.

865 Mellman, I., and Nelson, W.J. (2008). Coordinated protein sorting, targeting and distribution in polarized
866 cells. Nature reviews Molecular cell biology *9*, 833-845.

867 Mostov, K.E., Altschuler, Y., Chapin, S.J., Enrich, C., Low, S.H., Luton, F., Richman-Eisenstat, J., Singer,
868 K.L., Tang, K., and Weimbs, T. (1995). Regulation of protein traffic in polarized epithelial cells: the
869 polymeric immunoglobulin receptor model. Cold Spring Harb Symp Quant Biol *60*, 775-781.

870 Oyanadel, C., Holmes, C., Pardo, E., Retamal, C., Shaughnessy, R., Smith, P., Cortes, P., Bravo-Zehnder,
871 M., Metz, C., Feuerhake, T.*, et al.* (2018). Galectin-8 induces partial epithelial-mesenchymal transition with
872 invasive tumorigenic capabilities involving a FAK/EGFR/proteasome pathway in Madin-Darby canine
873 kidney cells. Mol Biol Cell *29*, 557-574.

874 Paladino, S., Lebreton, S., and Zurzolo, C. (2015). Trafficking and Membrane Organization of GPI-
875 Anchored Proteins in Health and Diseases. Curr Top Membr *75*, 269-303.

876 Paladino, S., Pocard, T., Catino, M.A., and Zurzolo, C. (2006). GPI-anchored proteins are directly targeted
877 to the apical surface in fully polarized MDCK cells. J Cell Biol *172*, 1023-1034.

878 Paladino, S., Sarnataro, D., Pillich, R., Tivodar, S., Nitsch, L., and Zurzolo, C. (2004). Protein
879 oligomerization modulates raft partitioning and apical sorting of GPI-anchored proteins. J Cell Biol *167*,
880 699-709.

881 Panakova, D., Sprong, H., Marois, E., Thiele, C., and Eaton, S. (2005). Lipoprotein particles are required
882 for Hedgehog and Wingless signalling. Nature *435*, 58-65.

883 Parchure, A., Vyas, N., Ferguson, C., Parton, R.G., and Mayor, S. (2015). Oligomerization and
884 endocytosis of Hedgehog is necessary for its efficient exovesicular secretion. Mol Biol Cell *26*, 4700-4717.

885 Parchure, A., Vyas, N., and Mayor, S. (2018). Wnt and Hedgehog: Secretion of Lipid-Modified
886 Morphogens. Trends Cell Biol *28*, 157-170.

887 Peng, T., Frank, D.B., Kadzik, R.S., Morley, M.P., Rathi, K.S., Wang, T., Zhou, S., Cheng, L., Lu, M.M.,
888 and Morrisey, E.E. (2015). Hedgehog actively maintains adult lung quiescence and regulates repair and
889 regeneration. Nature *526*, 578-582.

890 Pepinsky, R.B., Zeng, C., Wen, D., Rayhorn, P., Baker, D.P., Williams, K.P., Bixler, S.A., Ambrose, C.M.,
891 Garber, E.A., Miatkowski, K.*, et al.* (1998). Identification of a palmitic acid-modified form of human Sonic
892 hedgehog. J Biol Chem *273*, 14037-14045.

893 Perez Bay, A.E., Schreiner, R., Benedicto, I., Paz Marzolo, M., Banfelder, J., Weinstein, A.M., and
894 Rodriguez-Boulan, E.J. (2016). The fast-recycling receptor Megalin defines the apical recycling pathway of
895 epithelial cells. Nature communications *7*, 11550.

896 Perez Bay, A.E., Schreiner, R., Mazzoni, F., Carvajal-Gonzalez, J.M., Gravotta, D., Perret, E., Lehmann
897 Mantaras, G., Zhu, Y.S., and Rodriguez-Boulan, E.J. (2013). The kinesin KIF16B mediates apical
898 transcytosis of transferrin receptor in AP-1B-deficient epithelia. EMBO J *32*, 2125-2139.

899 Petrov, K., Wierbowski, B.M., Liu, J., and Salic, A. (2020). Distinct Cation Gradients Power Cholesterol
900 Transport at Different Key Points in the Hedgehog Signaling Pathway. Developmental cell *55*, 314-327
901 e317.

902 Petrov, K., Wierbowski, B.M., and Salic, A. (2017). Sending and Receiving Hedgehog Signals. Annu Rev
903 Cell Dev Biol *33*, 145-168.

904 Pizette, S., Matusek, T., Herpers, B., Therond, P.P., and Rabouille, C. (2021). Hherisomes, Hedgehog
905 specialized recycling endosomes, are required for high level Hedgehog signaling and tissue growth. J Cell
906 Sci *134*.

907 Porter, J.A., Young, K.E., and Beachy, P.A. (1996). Cholesterol modification of hedgehog signaling
908 proteins in animal development. Science *274*, 255-259.

909 Rindler, M.J., and Traber, M.G. (1988). A specific sorting signal is not required for the polarized secretion
910 of newly synthesized proteins from cultured intestinal epithelial cells. J Cell Biol *107*, 471-479.

911 Rodriguez-Boulan, E., and Macara, I.G. (2014). Organization and execution of the epithelial polarity
912 programme. Nature reviews Molecular cell biology *15*, 225-242.

913 Rojas, R., and Apodaca, G. (2002). Immunoglobulin transport across polarized epithelial cells. Nature
914 reviews Molecular cell biology *3*, 944-955.

915 Sargiacomo, M., Lisanti, M., Graeve, L., Le Bivic, A., and Rodriguez-Boulan, E. (1989). Integral and
916 peripheral protein composition of the apical and basolateral membrane domains in MDCK cells. J Membr
917 Biol *107*, 277-286.

918 Sarnataro, D., Paladino, S., Campana, V., Grassi, J., Nitsch, L., and Zurzolo, C. (2002). PrPC is sorted to
919 the basolateral membrane of epithelial cells independently of its association with rafts. Traffic *3*, 810-821.

920 Sbrogna, J.L., Barresi, M.J., and Karlstrom, R.O. (2003). Multiple roles for Hedgehog signaling in zebrafish
921 pituitary development. Developmental biology *254*, 19-35.

922 Scheiffele, P., Peranen, J., and Simons, K. (1995). N-glycans as apical sorting signals in epithelial cells.
923 Nature *378*, 96-98.

924 Sezgin, E., Levental, I., Mayor, S., and Eggeling, C. (2017). The mystery of membrane organization:
925 composition, regulation and roles of lipid rafts. Nature reviews Molecular cell biology *18*, 361-374.

926 Shyer, A.E., Huycke, T.R., Lee, C., Mahadevan, L., and Tabin, C.J. (2015). Bending gradients: how the
927 intestinal stem cell gets its home. Cell *161*, 569-580.

928 Simmen, T., Nobile, M., Bonifacino, J.S., and Hunziker, W. (1999). Basolateral sorting of furin in MDCK
929 cells requires a phenylalanine- isoleucine motif together with an acidic amino acid cluster. Mol Cell Biol *19*,
930 3136-3144.

931 Simon, E., Aguirre-Tamaral, A., Aguilar, G., and Guerrero, I. (2016). Perspectives on Intra- and
932 Intercellular Trafficking of Hedgehog for Tissue Patterning. J Dev Biol *4*.

933 Simons, K., and Ikonen, E. (1997). Functional rafts in cell membranes. Nature *387*, 569-572.

934 Stewart, D.P., Marada, S., Bodeen, W.J., Truong, A., Sakurada, S.M., Pandit, T., Pruett-Miller, S.M., and
935 Ogden, S.K. (2018). Cleavage activates dispatched for Sonic Hedgehog ligand release. Elife *7*.

936 Tanaka, Y., Okada, Y., and Hirokawa, N. (2005). FGF-induced vesicular release of Sonic hedgehog and
937 retinoic acid in leftward nodal flow is critical for left-right determination. Nature *435*, 172-177.

938 Therond, P.P. (2012). Release and transportation of Hedgehog molecules. Curr Opin Cell Biol *24*, 173-
939 180.

940 Tukachinsky, H., Kuzmickas, R.P., Jao, C.Y., Liu, J., and Salic, A. (2012). Dispatched and scube mediate
941 the efficient secretion of the cholesterol-modified hedgehog ligand. Cell Rep *2*, 308-320.

942 Tuma, P.L., and Hubbard, A.L. (2003). Transcytosis: crossing cellular barriers. Physiol Rev *83*, 871-932.

943 Vyas, N., Goswami, D., Manonmani, A., Sharma, P., Ranganath, H.A., VijayRaghavan, K., Shashidhara,
944 L.S., Sowdhamini, R., and Mayor, S. (2008). Nanoscale organization of hedgehog is essential for long-
945 range signaling. Cell *133*, 1214-1227.

946 Vyas, N., Walvekar, A., Tate, D., Lakshmanan, V., Bansal, D., Lo Cicero, A., Raposo, G., Palakodeti, D.,
947 and Dhawan, J. (2014). Vertebrate Hedgehog is secreted on two types of extracellular vesicles with
948 different signaling properties. Sci Rep *4*, 7357.

949 Walton, K.D., and Gumucio, D.L. (2021). Hedgehog Signaling in Intestinal Development and Homeostasis.
950 Annual review of physiology *83*, 359-380.

951 Wang, E., Brown, P.S., Aroeti, B., Chapin, S.J., Mostov, K.E., and Dunn, K.W. (2000). Apical and
952 basolateral endocytic pathways of MDCK cells meet in acidic common endosomes distinct from a nearly-
953 neutral apical recycling endosome. Traffic *1*, 480-493.

954 Wang, Q., Asarnow, D.E., Ding, K., Mann, R.K., Hatakeyama, J., Zhang, Y., Ma, Y., Cheng, Y., and
955 Beachy, P.A. (2021). Dispatched uses Na(+) flux to power release of lipid-modified Hedgehog. Nature.

956 Zavros, Y., Orr, M.A., Xiao, C., and Malinowska, D.H. (2008). Sonic hedgehog is associated with H+-K+-
957 ATPase-containing membranes in gastric parietal cells and secreted with histamine stimulation. Am J
958 Physiol Gastrointest Liver Physiol *295*, G99-G111.

959 Zeng, X., Goetz, J.A., Suber, L.M., Scott, W.J., Jr., Schreiner, C.M., and Robbins, D.J. (2001). A freely
960 diffusible form of Sonic hedgehog mediates long-range signalling. Nature *411*, 716-720.

961 Zhou, D., Li, Y., Zhou, L., Tan, R.J., Xiao, L., Liang, M., Hou, F.F., and Liu, Y. (2014). Sonic hedgehog is a
962 novel tubule-derived growth factor for interstitial fibroblasts after kidney injury. J Am Soc Nephrol *25*, 2187-
963 2200.

964 Zurzolo, C., Le Bivic, A., Quaroni, A., Nitsch, L., and Rodriguez-Boulan, E. (1992). Modulation of
965 transcytotic and direct targeting pathways in a polarized thyroid cell line. EMBO J *11*, 2337-2344.

966 Zurzolo, C., Lisanti, M.P., Caras, I.W., Nitsch, L., and Rodriguez-Boulan, E. (1993).
967 Glycosylphosphatidylinositol-anchored proteins are preferentially targeted to the basolateral surface in
968 Fischer rat thyroid epithelial cells. J Cell Biol *121*, 1031-1039.

969 <

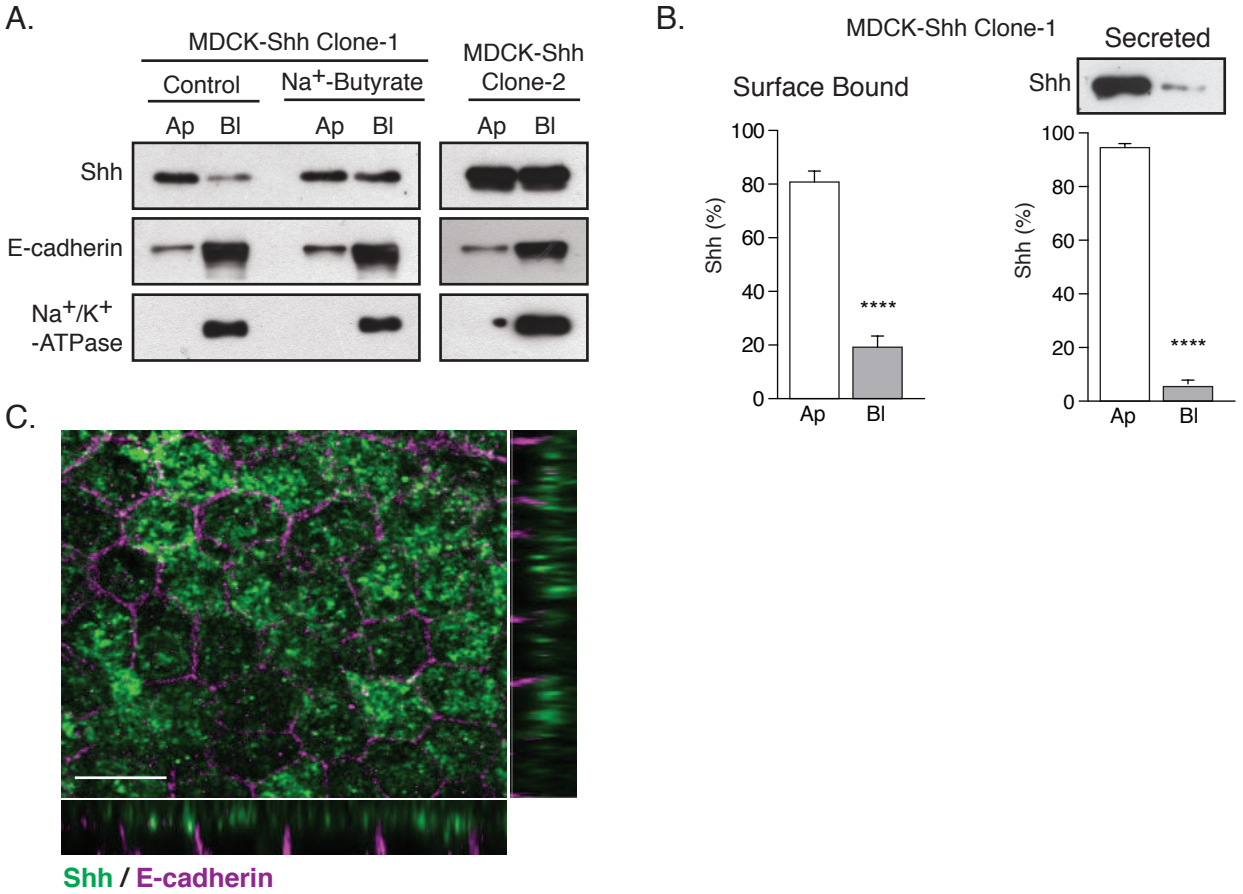

Figure 1. Shh expressed in MDCK cells is apically distributed and secreted. (A) Domain-selective biotinylation of permanently transfected MDCK-Shh grown in Transwell filters. MDCK-Shh Clone 1 shows Shh mainly at the apical cell surface or non-polarized when its expression is increased by 2mM Na+-butyrate treatment for 24h. MDCK-Shh Clone 2 expressing higher Shh levels displays Shh equally distributed among the apical and basolateral cell surface. The basolateral distribution of E-cadherin and Na+/K+-ATPase corroborates the polarized status of the cells in all conditions. (B) Graphs show Shh relative apical versus basolateral cell surface distribution and secretion in MDCK-Shh clone 1. Domain-specific cell surface biotinylation of six independent experiments (n=6) and immunoblot of TCA precipitated proteins from low-serum media conditioned for 6 h of three independent experiments (n=3) reveal aprox. 80% apical cell surface distribution and more than 90% secretion of Shh, respectively. Data expressed as a percentage of total surface or secreted Shh and analysed by an unpaired t-test. In all figures error bars represent mean ± SEM. ****, P≤0.0001. (C) MDCK-Shh clone 1 cells immunofluorescence staining for Shh (green) and E-cadherin (magenta). Images displayed as maximum projection of confocal z-stack and orthogonal views show an apical pattern of Shh. Scale bar, 10 µm.

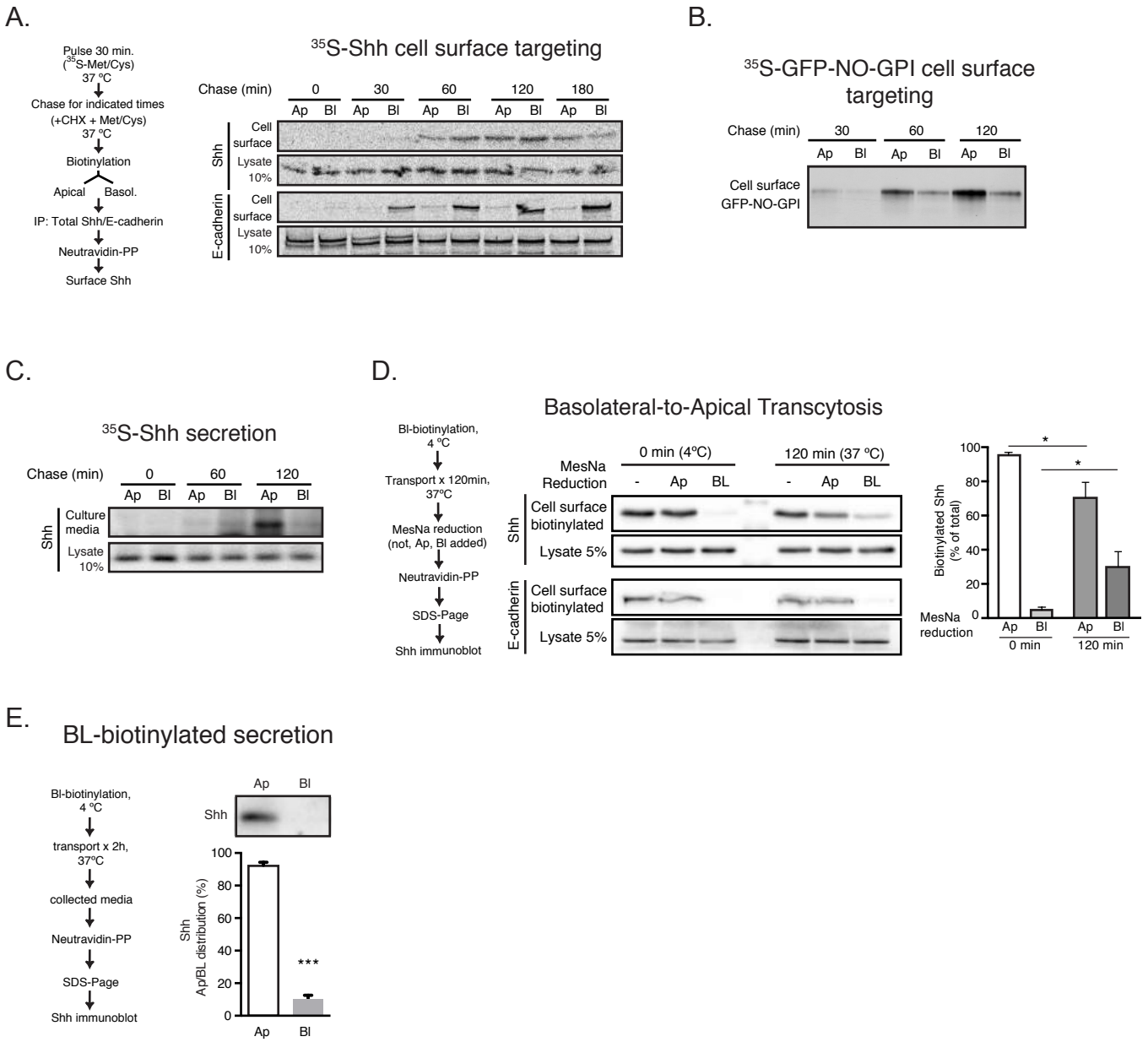

Figure 2. Newly synthesized Shh first arrives at the basolateral cell surface and then reaches the apical side by transcytosis for secretion. Polarized monolayers grown in Transwell filters of MDCK-Shh (A, C) or GFP-NO-GPI (B) cells were pulse-labeled with ^{35}S-methionine/cysteine and chased at 37°C for the indicated times by subsequent cell-surface-specific biotinylation at 4°C. Cell surface targeting of newly synthesized proteins (Shh, E-cadherin or GFP-NO-GPI) and loading control (10% of total protein in lysates) was analyzed by SDS-PAGE and Cyclone radioactivity scanner (see details in Materials and Methods). (C) Immunoprecipitation of ^{35}S-Shh shows its secretion to either apical or basolateral chambers. (D) MDCK-Shh were incubated with reducible-Biotin by the basolateral domain at 4°C, then allowed to resume trafficking by incubation at 37°C for 120 min. Biotin was then reduced by either apical or basolateral sides to detect internalization or transcytosis of the pool of Shh initially biotinylated by the basolateral domain. E-cadherin was used as a control of a basolateral resident protein. Data expressed as a percentage of total surface Shh of three independent experiments (n=3) and analyzed by an unpaired t-test. In graph error bars represent mean ± SEM. *, P≤0.05. (E) MDCK-Shh cells were biotinylated from the basolateral side at 4°C and then incubated at 37°C for 2h. Apical and basolateral conditioned media were collected, precipitated with Neutravidin and analyzed by immunoblot for secreted Shh. Data expressed as a percentage of total secreted Shh of four independent experiments (n=4) and analyzed by an unpaired t-test. In graph error bars represent mean ± SEM. ***, P≤0.0001.

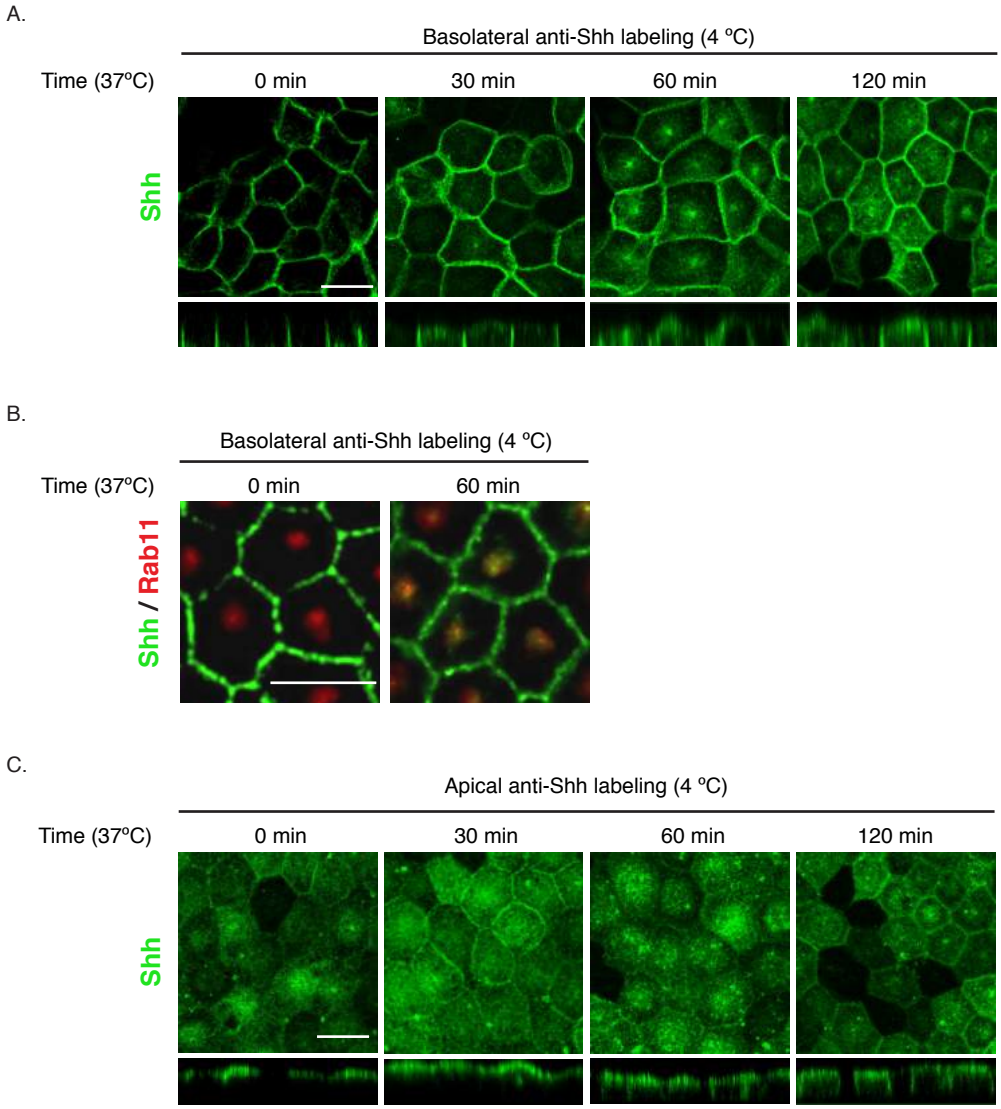

Figure 3. Basolateral Shh moves to the apical side by transcytosis through Rab-11-ARE and apical Shh can undergo reverse transcytosis. MDCK-Shh cells grown in Transwell filters were incubated with anti-Shh antibodies at 4ºC from the basolateral (A, B) or apical (C) sides, shifted 37ºC for the indicated times and Shh distribution was followed by immunofluorescence and orthogonal views of confocal images. Shh moved from the basolateral to the apical domain involving a subapical punctate compartment typical of the ARE, as corroborated in by its colocalization with endogenous Rab11 (red) after 60 min of trafficking (B). (C) Apically immunolabeled Shh moving to the basolateral domain is detectable after 60 min. Scale bar, 10 µm.

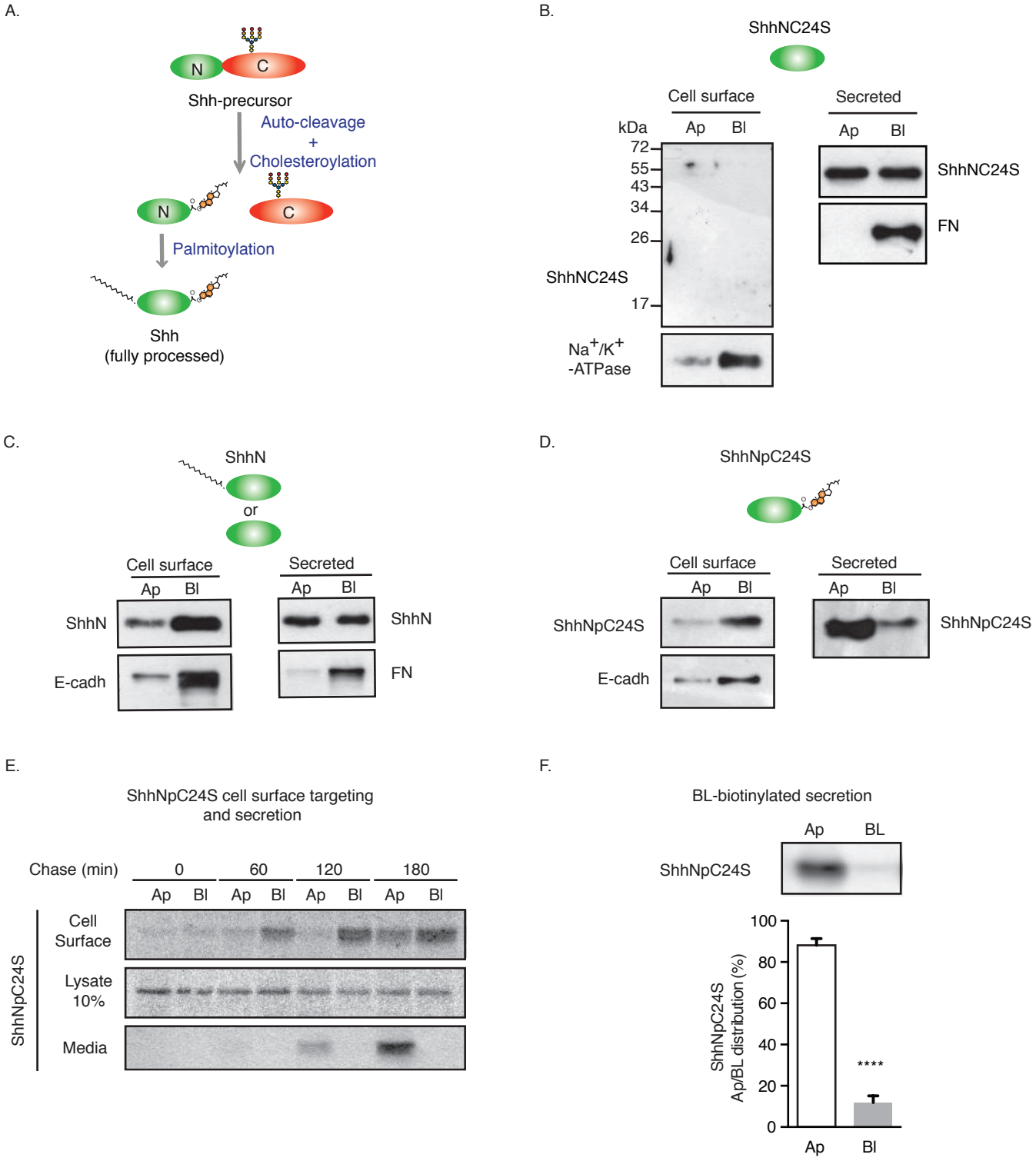

Figure 4. Sorting of Shh lipidation mutants. (A) Schematic illustration of Shh processing and lipidation. (B-F) MDCK cells stably expressing Shh lipidation mutants lacking both lipids (B, ShhNC24S), containing only palmitoyl (C, ShhN) or cholesteryl (D-F, ShhNpC24S) moieties were analyzed by domain-specific cell-surface biotinylation and secretion (presence in the media after 2h accumulation, TCA precipitation and immunoblot). Basolateral E-cadherin and Na+/K+-ATPase transmembrane proteins and secreted Fibronectin (FN) were used to control polarity. (E) MDCK-ShhNpC24S cells were pulsed labeled with ^{35}S-methionine/cysteine and chased to detect protein arrival to each cell surface along with its polarized secretion, as in Figure 2A. Samples were analyzed by SDS-PAGE and Cyclone radioactivity scanner. (F) MDCK-ShhNpC24S cells were biotinylated from the basolateral side at 4°C and then incubated at 37°C for 2h. To assess for ShhNpC24S secretion, apical and basolateral conditioned media were collected, precipitated with Neutravidin and analyzed by immunoblot. Data expressed as a percentage of total secreted Shh of three independent experiments (n=3) and analysed by an unpaired t-test. In graph error bars represent mean ± SEM. ****, P≤0.0001.

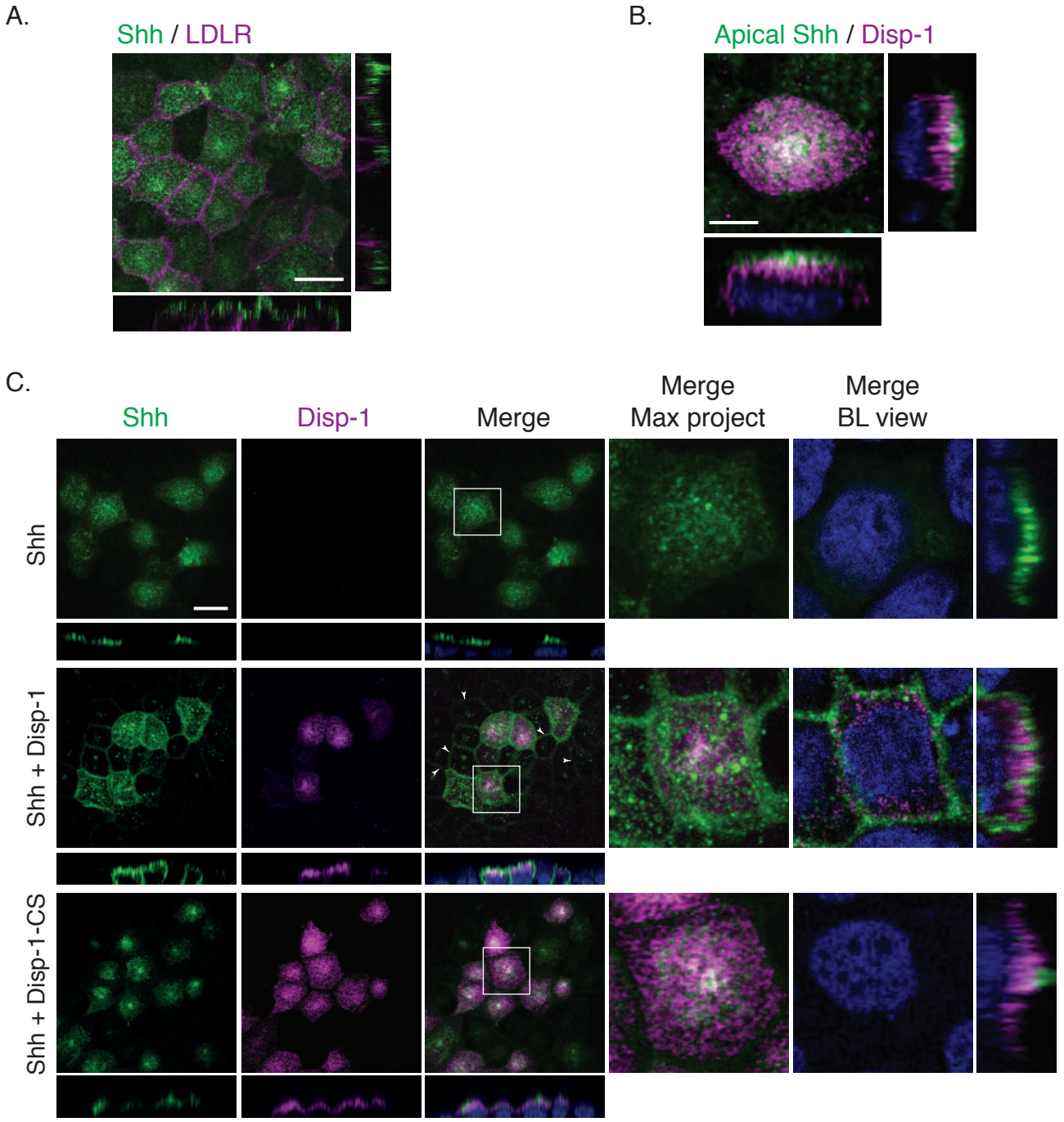

Figure 5. Shh is apically and basolateraly distributed under Dispt-1 expression while it is retained at ARE in cells expressing cleavage deficient Disp-1CS. MDCK cells were plasmid microinjected and protein expression was allowed for 4h. (A) Immunofluorescence of co-microinjected Shh (green) and basolateral marker LDLR-GFP-Y18A (magenta). (B) Co-microinjected cells with Shh and Disp-1 were fixed and immune-stained first by the apical side with anti-Shh (green) antibodies and then permeabilized and stained for Disp-1 with anti-HA (magenta) antibodies. (C) Cells were microinjected with Shh alone (upper panels) or together with Disp-1 (middle panels) or cleavage deficient Disp-1-CS (lower panels). Then cells were analyzed by indirect immunofluorescence for Shh (green) and Disp-1 (HA, magenta). Arrowheads indicate non-microinjected cells with basolateral Shh localization due to secretion from expressing cells. Zoomed image to the right demonstrates Shh apically and basolaterally detected in the presence of Disp-1 (BL view) or retained in the ARE compartment in the presence of Disp-1-CS (maximal projection, also see Fig. 7). In all figures scale bar, 10 µm.

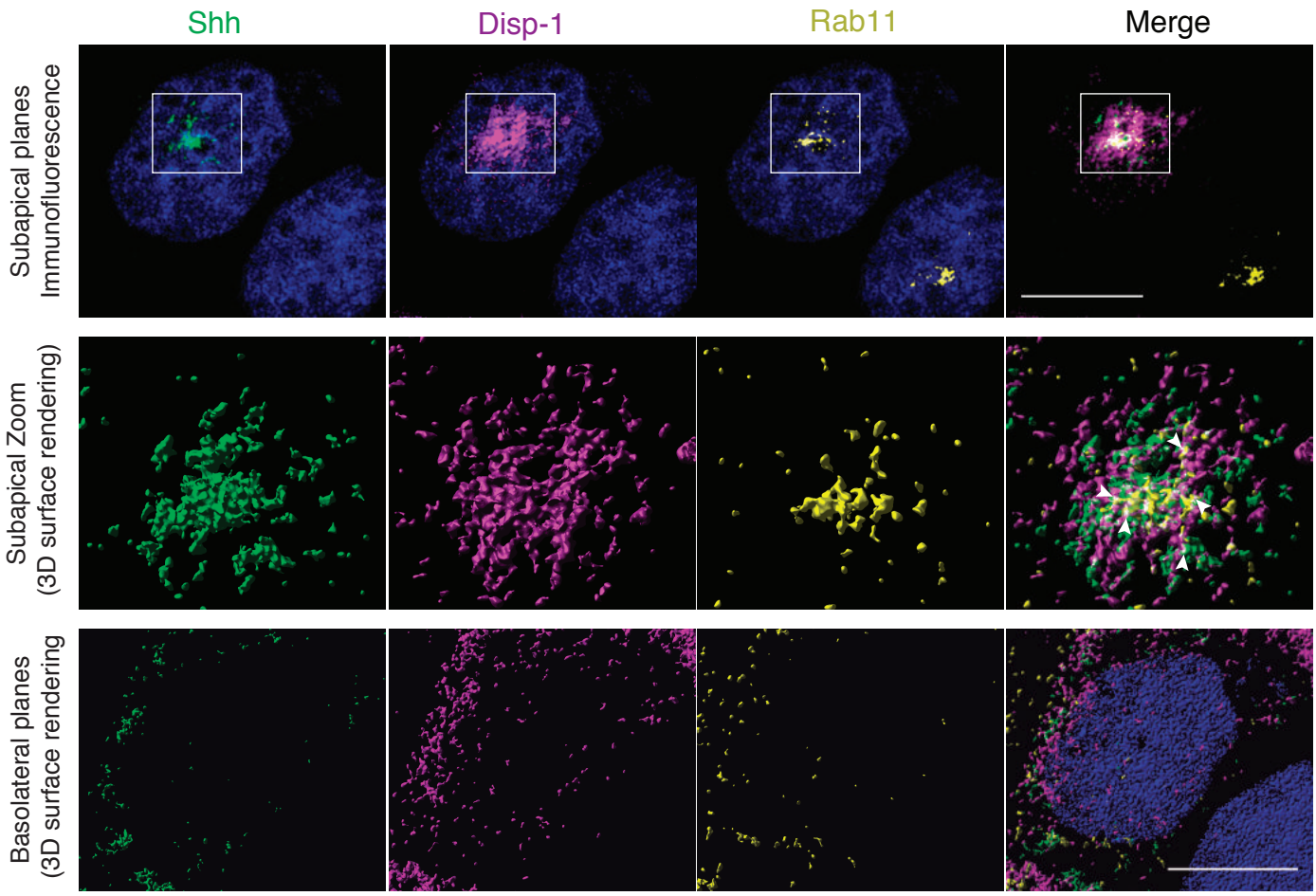

Figure 6. Colocalization of transiently expressed Shh and Disp-1 in Rab11-ARE. Polarized MDCK cells were microinjected with Shh-GFP (green) along with Disp-1 and after 4 hrs expression cells were fixed and immunostained for anti-HA (magenta) and anti-Rab11 (yellow). A microinjected cell is shown in the upper panel (center) and a non-microinjected cell is visible at the down-right corner. Maximal projection of 10 planes of 0.1 microns sections over thshows the 3D surface rendering of the zoomed region, in which colocalization of Shh (green) Disp-1 (magenta) e nucleus shows the subapical Rab11-ARE displaying a tubular pattern. Center panel and Rab11 (yellow), is shown by white arrowheads. The lower panel illustrates a 3D surface rendering of medial and basal planes (40 planes of 0.1 microns sections), in which basal distribution of Disp-1 and few vesicles containing Shh or Rab11 are shown. Scale bar, 10 µm.

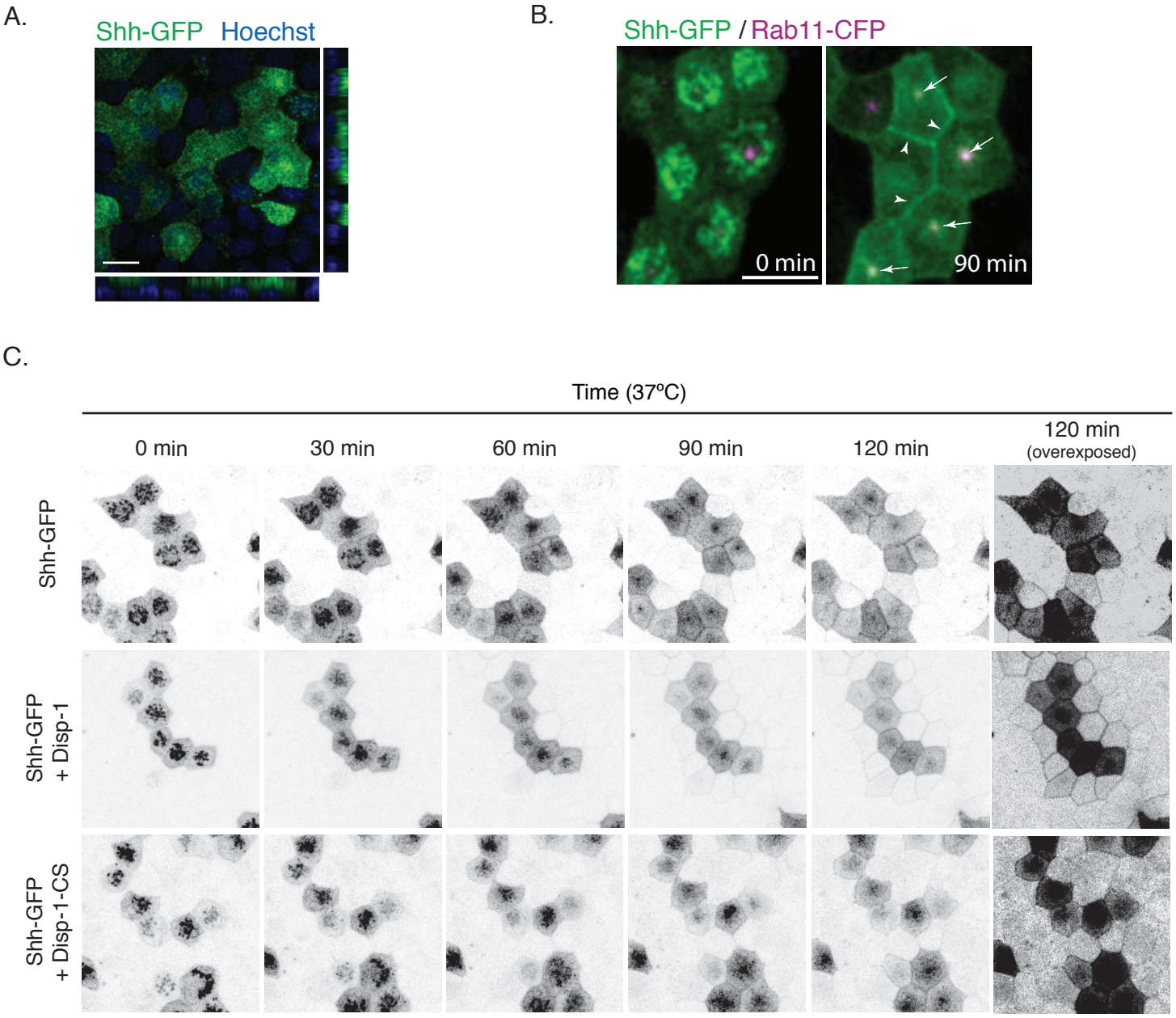

Figure 7. Basolateral secretion of Shh from the TGN is enhanced by Disp-1 and decreased by Disp-1-CS. (A) Shh-GFP distribution after 4 h of expression in plasmid microinjected polarized MDCK cells show a similar polarity as Shh at steady state (See Figure 1). (B) Shh-GFP expressed by microinjection in MDCK cells permanently transfected with Rab11-CFP plasmid. After 45 min of Shh-GFP expression, the cells were incubated for 2 h at 20ºC to arrest the protein at the TGN (time = 0) and then shifted to 37ºC to reestablish the exit from TGN for 90 min. Arrows point to Rab11-ARE and arrowheads show basolateral Shh-GFP. (C) Live cell imaging analysis of Shh-GFP trafficking from the TGN to the cell surface for the indicated times. Shh-GFP alone (upper panel), co-microinjected with Disp-1 (middle panel) or Disp-1-CS (lower panel). Shh-GFP detected in the border of neighboring non-expressing cells reflects its basolateral secretion, which is enhanced by co-expressed Disp-1 and decreased by Disp-1-CS, more clearly seen in the overexposed image at time 120 min.